UNIVERSITY OF OKLAHOMA

GRADUATE COLLEGE

HYDROGEOCHEMISTRY OF A HETEROGENEOUS AQUIFER LOCATED IN UNAWEEP CANYON, MESA COUNTY, WESTERN COLORADO

A THESIS

SUBMITTED TO THE GRADUATE FACULTY

in partial fulfillment of the requirements for the

Degree of

MASTER OF SCIENCE

By

JOY FOLUSO
Norman, Oklahoma 2021

HYDROGEOCHEMISTRY OF A HETEROGENEOUS AQUIFER LOCATED IN UNAWEEP CANYON, MESA COUNTY, WESTERN COLORADO

A THESIS APPROVED FOR THE
SCHOOL OF GEOSCIENCES

BY THE COMMITTEE CONSISTING OF

Dr. Kato T. Dee, Chair

Dr. Andrew S. Elwood Madden

Dr. Gerilyn S. Soreghan

Dr. Michael Behm

ACKNOWLEDGEMENTS

First and foremost, I would like to appreciate Dr. Dee for first accepting me as a graduate student here at OU and for his guidance throughout my graduate program. I really do appreciate all your effort and hard work at trying to instill knowledge in me and helping me become a better scientist. I would also love to appreciate my other committee members Dr. Michael Behm, Dr. Gerilyn (Lynn) Soreghan and Dr. Andrew S. Elwood Madden for all their help and support along the way during this process.

I would also like to thank Chelsey Gallagher who helped me collect samples and for allowing me text her at 1am for random things. I also appreciate her for her doggedness, and I apologize for getting bitten by a spider because we were trying to find one of my sampling sites.

I would like to thank Fred and Amy Bolton, as well as the Moore's for allowing me on their property to sample their wells even with Covid. D. I would love to appreciate Dr. E for helping me out even with his busy schedule

I would like to appreciate my friends: Inioluwa, Judah, Bunmi, Chinasa, Tomi, Brandy, Tunde and many more for always checking in on me and assisting me in on way or the other. Thank you to the Geochem group who listened to me babble during presentations but still provided support and guidance throughout my two years at OU.

Finally, I would love to thank God for being my all in all.

Table of Contents

Abstract

The intersection of an increasing population, climate change, pollution, and over allocation of water continue to place additional strain on groundwater resources in arid regions. Groundwater in arid environments is particularly susceptible to overuse, and therefore a thorough understanding of groundwater sources and its contribution to sensitive ecosystems is vital. Unaweep Canyon, in the arid region of Colorado's western slope, is a geologically unique site that harbors a buried paleovalley. The modern valley contains up to ~500 m of sediment fill comprising unconsolidated lacustrine, fluvial, and mass-wasting deposits, as well as possible lithified sedimentary rocks. We hypothesize that the unconsolidated layers in Unaweep Canyon aquifer are not hydro-geochemically linked and represent different, unique sources of groundwater. Our study focused on integrating published geologic information, geophysical data, and seasonal geochemical properties of groundwater and surface water to delineate multiple sources of water for both human and ecosystem needs. Several streams, seeps, Precambrian bedrock spring aquifers, and several domestic wells were sampled for metals, anions, and stable isotopes (^{18}O and ^{2}H) during spring, summer, and fall 2020 to identify seasonal effects. Piper plots also revealed that the Precambrian bedrock spring aquifers may be a sodium chloride or mixed type water, the spring is a sodium chloride type water, and the surface and groundwaters are magnesium-bicarbonate type waters. Furthermore, the isotopic composition of the seeps, West Creek, domestic well and Precambrian bedrock samples range from -14.06 to -15.16‰ $\delta^{18}O$ and -103.5 to -109.46‰ $\delta^{2}H$, -12.89‰ to -14.7‰ $\delta^{18}O$ and -99.3 to -106.68‰ $\delta^{2}H$, -13.64 to -14.77‰ $\delta^{18}O$ and -102.4 to -105.94‰ $\delta^{2}H$, -14.27 to -15.39‰ $\delta^{18}O$ and -108.7 to -112.78‰ $\delta^{2}H$ respectively. Principal Component Analysis coupled with Spearman Correlation supported the existence of seasonal variation and multiple groundwater sources from all the sampling locations. Seasonal variability amongst in-situ water

chemistry, metal and stable isotope results were attenuated, likely attributable to the drought conditions of 2020. Our results suggest the presence of multiple sources of groundwater within Unaweep Canyon, leading for the potential to utilize each source in a sustainable fashion. The findings and methodology used in our study may have applicability in similar hydrogeologic settings where alternate water sources.

List of Figures

List of Tables

1. INTRODUCTION

1.1 Water in arid environments

Groundwater has been recognized as one of the most valuable natural resources in all climatic regions of the world because it is the primary source of water used in meeting the domestic needs of about one-third of the world's population (Sefie et al., 2015, United Nations Environment Program, 1999). During the last few decades, the steady increase in the global demand for groundwater due to an increase in population poses a threat to the sustainable development of human society (Mekonnen and Hoekstra, 2016). In addition, climate change has exacerbated groundwater demand in arid and semi-arid regions.

Arid and semi-arid regions (with mean annual precipitation of 25-500 mm) composes one-third of the total land area on earth and are inhabited by at least 400 million people (Williams, 1999). In the United States, arid regions prevail from about the middle the Great Plains and extends across the Rocky Mountains to the Pacific Ocean in states such as Colorado, Utah, and Arizona to mention a few (Powell, 1879). These areas like other parts of the United States have a high strain placed on available groundwater resources by the increase in population and groundwater in these arid environments is further threatened by more prevalent factors such as climate change, pollution and over-extraction (Williams, 1999). As a result, such regions are incredibly prone to overuse of water resources if not managed properly and this strain in turn affects sensitive ecosystems including wetlands that rely on groundwater, thus creating the need to identify various sustainable sources of potable water for humans.

1.2 Non-Invasive Methods in Sourcing Groundwater in Snow-Dominated Watersheds

Snow-dominated watersheds are especially susceptible to climate change yet represent key sources of water for one sixth of the world's population ((IPCC, 2014, MRI, 2015, Mankin et al., 2015). Groundwater sourced from deeper aquifers experiences little to no immediate effects of climate change and can help provide a more dependable water supply to help against climate extremes (Taylor et al., 2013). Traditionally, characterization of groundwater and its properties including flow pathways typically includes the installation of wells or piezometers in the area of interest, but this is expensive and may perturb the natural hydrogeological environment (Wang et al., 2015, Rizzo et al., 2004, Maineult et al., 2008). However, more recently, non-invasive methods are becoming more common in studies focusing on characterizing aquifers. These methods are generally cost-effective and produce adequate data on the presence and source of water in the aquifer. Common non-invasive techniques include general water chemistry, stable isotopes, trace metals, Rare Earth Element (REE) patterns and geophysical methods (e.g. seismic and resistivity) to locate and differentiate between shallow and deep aquifers.

1.2.1 Application of Water Chemistry, Stable Isotopes and REE to Evaluate Groundwater Sources.

Solute chemistry is influenced by variations in meteoric precipitation, evapotranspiration, dissolution-precipitation reactions, mineral weathering, or mixing processes (Carrillo-Rivera et al., 2007) and thus produce spatial and seasonal changes in groundwater and surface water chemistry (Matthess, 1982). These solutes include dissolved ions such as Ca^{2+}, Mg^{2+}, SO_4^{2-}, dissolved organic carbon (DOC), trace metals (e.g U^{+}, B^{+}) and REEs (e.g Y, Ce, Eu). The dissolved ions in both surface and groundwater are extremely useful in hydrogeochemical studies because these ions are typically indicative of dissolution or weathering processes which leads to the release of ions

from the geologic material the water contacts. For example, in a study carried out in Delhi, India, Kumar et al. (2006) observed excessive Na^+ in groundwater relative to the surface water in the Yamuna river. The excessive Na^+ was then linked to the dissolution of silicates in the aquifer. Nonetheless, Zhou et al. (2014) observed that surface water/ shallow groundwater interactions result in surface water exhibiting similar water chemistry as groundwater (Zhou et al., 2014). In contrast to shallow aquifers, groundwater originating from deep aquifers commonly exhibit higher concentrations of dissolved ions owing to prolonged water-mineral interactions ((Hazen et al., 2002, Marks et al., 2008, Walton-Day and Poeter, 2009, Sefie et al., 2015, Abd El Samei and Sadek, 2001, Abdelshafy et al., 2019).

The use of variation in water chemistry as a result of the water's source has been harnessed by water resource management studies as fingerprints that can be harnessed to identify different groundwater sources in arid-semi/arid regions. This typically involves the use of Piper diagrams in identifying geochemical facies and therefore, classify water samples by source. In a study in the Dharapuram area, a semi-arid region in India, Kumar (2016) utilized the hydrogeochemical data of groundwater samples to plot a Piper trilinear diagram which identified three water types, Na–Cl, Ca–Cl and mixed Ca–Mg-Cl type. A study by Aly et al. (2013) in an arid region in Kingdom of Saudi Arabia (KSA), revealed two water types: A Na-Cl-SO_4 and Ca-Mg-SO_4, signifying two different sources of groundwater in the area.

However, the use of water chemistry alone to determine water source is not very reliable because factors such as changes in concentrations along flow paths due to biologically mediated reactions in places such as wetlands can alter water chemistry Chapman et al. (2003); but it can be used in conjunction with other hydrogeochemical analysis such as stable isotopes. Such biologically mediated reactions include the amelioration of water chemistry which occurs during

the process of wetlands retaining nitrogen via sorption and incorporating it into biomass, and denitrification which removes Nitrogen, thus reducing Nitrogen loads flowing into surface water (Costanza et al., 1998, Zedler et al., 2003). For remediation processes, such biologically mediated processes can help the ecosystem at large; however, it alters the water chemistry greatly and can therefore complicate attempts to trace the origin of the water feeding the wetland.

Nonetheless, stable isotopes of O and H such as ^{18}O and ^{2}H are widely used to assess chemical and physical properties associated with groundwater that are a factor of temperature, altitude, evaporation, etc. (Chacko et al., 2001). Their wide use is because ^{18}O and ^{2}H are the most common isotopes in water and also, their conservative nature help to provide a useful and increasingly applied tool for understanding hydrological processes across various scales, including identifying the origins of water in various environments, such as mountainous, fractured-rock environments and semi-arid to arid regions (Barbieri et al., 2005, Chapman et al., 2003, Coplen et al., 2000, Hazen et al., 2002, Walton-Day and Poeter, 2009, McDonnell and Beven, 2014). Isotopic signatures of water are generally conservative in groundwater over short time periods, but at the surface they can be altered due to fractionation caused by evaporation (Clark and Fritz, 1997). In arid environments, evaporation from a shallow water table is quite common and can be used to distinguish between shallow and deeper groundwater (Yin et al., 2011). Shaw et al. (2017) were able to distinguish between shallow groundwater, springs, and surface water, where the springs exhibited depleted ^{18}O isotopic signatures relative to the shallow groundwater and the surface water which had strong evaporated isotopic signatures (enriched in ^{18}O). However, isotopes can experience extreme seasonal fluctuations thus creating the need to combine this approach with other geochemical methods for higher accuracy in the results of such studies (Gurrieri and Furniss, 2004).

Studies have also combined the use of general water chemistry, ^{18}O and ^{2}H isotopes to distinguish between various sources of water. In a study carried out in South Park Colorado; Chapman et al. (2003) attempted to identify the water source supplying high-altitude wetlands (fens) in the area using isotopic and water chemistry analysis. The variation in the isotopic signatures of the groundwater samples obtained signified the presence of a deeper aquifer which was observed to be isotopically depleted in relation to heavier isotopes when compared to the shallow groundwater and surface water in the area. Further geochemical modeling using the general water chemistry (such as concentrations of Ca^{2+}, Mg^{2+}) and isotopic data demonstrated the source of the water feeding the fens to be the shallow groundwater. In China, Han et al. (2009), through the use of Piper plots of the major ions were able to identify three water types, $HCO_3.SO_4$-Na, HCO_3-Ca and $HCO_3.SO_4$-Ca.Mg in the arid-semiarid Xinzhou Basin. The result of the water chemistry data corroborated the isotopic signatures, revealing three water sources: surface water, a shallow and a deeper aquifer system. However, in areas with contrasting mineralogy, the use of seasonality in REE fingerprints of the host rock due to its special rock-water interactions (Tweed et al., 2006, Playà et al., 2007).

Aquifer-rock interactions can produce unique REE patterns that serve as groundwater tracers (Banner et al., 1989, Smedley, 1991). REE are generally separated into light and heavy REE (LREE and HREE, respectively) where REEs with an atomic number lower than Eu (63) are considered LREE while Gd (64) and any REE with a higher atomic number are classified to be either MREE or HREE (Castor and Hendrick, 2006). By classifying REE based on their atomic number, a simplified description and possible quantification can be made between interelement relationships. Certain anomalies that occur in unique REEs as a result of redox especially for Ce and Eu (Brookins, 1989) and anthropogenic emissions for Gd (Bau and Dulski, 1996) can assist in

interpreting geochemical processes. Johannesson et al. (1997) observed that carbonate rock aquifers exhibited negative Ce anomalies, depletions in the LREEs, enrichment in the MREEs and HREE whereas the opposite occurred in the water samples originating from felsic volcanic aquifers of south-central Nevada. They suggested that the patterns of REEs in these groundwaters are controlled greatly by a combination of solution complexation by carbonate ions and adsorption onto O-donor surfaces. However, such factors controlling/influencing geochemical reactions and ultimately altering REE fractionation patterns in groundwater has not yet been fully understood and thus can limit the use of REE in hydrogeochemical studies. Also, the use of REE can be plagued by values below the detection limit of the analytical method (Palarea-Albaladejo et al., 2014, Noack et al., 2014).

1.2.2 Seasonality in Water chemistry, Stable Isotopes and REE.

General water chemistry has been shown to vary seasonally which is linked to nutrient cycling in the environment driven by the hydrologic cycle (Mulholland and Hill, 1997, Walton-Day and Poeter, 2009). Differences in water chemistry can then be used to infer the processes that have occurred over time. In mountainous environments, as snowmelt travels through the subsurface, it accumulates solutes that are released through various processes such as chemical weathering and the breakdown of organic matter (Winnick et al., 2017) and provides further insight into surface water, groundwater and bedrock interactions (Anderson et al., 1997, Kim et al., 2017, Carroll et al., 2018). Various studies have used the concentration-discharge (C-Q) relationships of solutes to provide useful information on hydrologic processes and interactions with solute generation at large spatial scales (Winnick et al., 2017, Carroll et al., 2018, Dwivedi et al., 2018). Solute concentration and increasing flow vary inversely for both groundwater and surface water (Hornberger et al., 2001, Scanlon et al., 2001, Godsey et al., 2009). In surface water, base cations

(Ca^{2+}, Mg^{2+}, K^{+} and Na^{+}) decrease with increasing discharge during snowmelt periods whereas increasing concentrations occur during winter base flow periods (Carroll et al., 2018). Shallow groundwater also tends to have slight variations in solute concentration in different seasons but not to the same degree as surface water (Imes and Wood, 2007, Ameli et al., 2015). However, deep confined groundwater flow often results in relatively consistent water chemistry throughout the year (Walton-Day and Poeter, 2009). The lack of variation in water chemistry in deeper aquifers is typically as a factor of residence time and the confining layer that separates it from the shallow aquifer below it and acts as barrier that prevents the inflow of water (Chapagain et al., 2009, Exner-Kittridge et al., 2016, Shakya et al., 2019).

The comparison of solute concentrated and diluted surface water and possibly, shallow groundwater, observed due to seasonal changes has been used to distinguish between various water sources. Sacks et al. (1992) demonstrated seasonality in Lake Santa Olalla, France where in the dry season, the surface water was solute concentrated and in the wet season became solute diluted, whereas the shallow groundwater was fairly conservative in areas where it was not being recharged by the lake. In the East River watershed (Colorado), snowmelt/solute relationships have been widely studied (Carroll et al., 2018, Winnick et al., 2017). In surface water, Winnick et al. (2017) demonstrated that solute fluxes were prevalent, with the concentrations of solute (such as HCO^{-}_{3} and SO^{2-}_{4}) much lower during snowmelt conditions and greater during baseflow. Carroll et al. (2018) identified seasonal variations in the solute concentrations of surface water and shallow groundwater, but in the deeper groundwater, the solute concentration was quite consistent. Thus, showing that seasonal effects observed in general water chemistry can be a valuable tool in identifying different water sources.

Stable isotopes are another hydrochemical component of water commonly used to delineate seasonal interactions between groundwater and surface water and even relative age differences (young versus old) of groundwater. This involves the use of stable isotopes of water: ^{18}O and ^{2}H (Maréchal and Etcheverry, 2003, Gurrieri and Furniss, 2004). In mountainous environments, isotope distribution is strongly controlled by snowmelt, evapotranspiration, and temperature (Fontes, 1980, Mazor, 1991, Gat, 1996, Clark and Fritz, 1997, Gibson et al., 2005, Li et al., 2019, Soderberg et al., 2013, Farid et al., 2015). Evaporation of surface water leads to an enrichment of heavier isotopes whereas precipitation (including snowmelt) results in depletion of the heavier isotopes (Clark and Fritz, 1997, Walton-Day and Poeter, 2009). Typically, the isotopic composition of water in deep subsurface aquifers are constant over short time scales but can change over long time scales through geothermal exchange and water-rock interactions (Clark and Fritz, 1997). However, certain mountainous shallow aquifers have shown limited seasonal variations except for a depletion in the heavier isotope due to snowmelt (Walton-Day and Poeter, 2009). In a study by Zhao et al. (2018), enrichment of the heavier isotope during the dry season and depletion of the heavier isotope during the wet season was used to differentiate between surface water, shallow groundwater and a deeper groundwater source in the Heihe River Basin, northwestern China which is located in an arid to semi-arid environment. However, shallow aquifers can experience seasonal variations and thus be used to distinguish shallow and deeper aquifers. In the Ordos Plateau, a semi-arid region located in the eastern part of Northwest China, Yin et al. (2011) also differentiated shallow and deeper groundwater due to the effects of evaporation that caused the shallow groundwater samples to be enriched in the heavier isotopes whereas the deeper groundwater experienced little to no seasonal variation in isotope composition. Walton-Day and Poeter (2009) also demonstrated the usefulness of the influence of seasons on isotopic data in

understanding the sources of water to the Dinero mine tunnel located in Turquoise lake, Leadville Colorado. The surface water samples were isotopically heavier during snowmelt (spring), lighter in the summer months and heavier during baseflow conditions, which differed from other water samples analyzed in the study area. The deep groundwater was enriched in ^{18}O whereas the Dinero water was a combination of deep groundwater and shallow groundwater recharged by seasonal snowmelt.

In complex geological settings and complex mineralogy, seasonal REE patterns in water have also been used for differentiating between surface water and groundwater (Duvert et al., 2015). The collection of temporal data is important because samples collected in only one season fail to adequately represent a system that changes seasonally (Shiller, 1997). Studies have also shown surface water chemistry to fluctuate greatly over time and seasons (Ingri et al., 2000, Shiller, 2002, Bagard et al., 2011, Möller et al., 2014). While for shallow groundwater, a range of responses to seasonality has been identified, ranging from its REE concentrations having no seasonal variation in concentration to there being substantial differences (Gruau et al., 2004, Pourret et al., 2009, Poh and Gasparon, 2011). In mountainous areas where systems can be highly responsive to seasonal changes, Duvert et al. (2015) utilized seasonal variation in REE abundances and normalized patterns in water samples to characterize the different aquifer systems in the Teviot Brook catchment (Southeast Queensland, Australia). The results showed contrasting variation in the REE concentrations of both surface water and shallow groundwater, while in igneous rocks, the REE concentrations showed no variation between seasons.

1.2.3 Shallow Geophysical Methods

Shallow geophysical methods such as Electrical Resistivity Method (ERM) and 2D seismic acquisition have been used in groundwater exploration to delineate subsurface stratigraphy

(Riwayat et al., 2018, Patterson, 2019, Behm et al., 2019) and these methods can be used in conjunction with hydrogeochemical studies to confirm the presence of groundwater in an area. For example, in Unaweep canyon, Patterson (2019) utilized 2D seismic acquisition to delineate the Precambrian basement geometry. Pre-stack migration results showed an upper reflector (with a profile between 600-1200 m and an elevation of 1845 – 1945m) with a velocity of 1500m/s which is the velocity of saturated sand (Wightman et al., 2003). The upper reflector indicated the relative location of the water table (Patterson, 2019), but further confirmation is needed. The interval and stacking velocities showed four distinct velocity layers which have been interpreted as four stratigraphic units. The first layer was interpreted to be saturated sand (or the fanglomerate), the second, lacustrine sediments, the third possibly lithified sedimentary rocks and finally the metamorphic Precambrian basement being the fourth layer. Generally, the upper ~half of the geophysical observations tie in closely with core data retrieved from an up-canyon site previously (Marra, 2008).

1.3 General Research Scope: Objectives and Hypotheses

Mesa County, Colorado, U.S.A., is a semi-arid region with an estimated 92% population increase from 2000 to 2025 (Mesa County, 2019) that will likely strain the county's water resources. Unaweep Canyon, located within Mesa County, is a geologically unique site with an inferred (buried) over-deepening hypothesized to be a result of initial valley formation by glaciation (possibly in the Paleozoic), and there might therefore be lacustrine strata of Paleozoic age in the overdeepened section but further investigation would be needed to confirm this.As evidenced by well and core log data from the canyon, there are possibly two or more aquifers present in Unaweep Canyon (Marra, 2008, Soreghan et al., 2009). The upper, shallow aquifer is an alluvial aquifer, composed of sediments accumulated primarily through continuous mass

wasting of the valley walls. The other aquifers are inferred from core data and geochemical results from previous sampling efforts in March and September 2018 which hinted at probable multiple sources of groundwater. Thus, to confirm the presence of various sources of groundwater originating from multiple aquifers within Unaweep Canyon, I hypothesize that:

1. The Unaweep Canyon aquifer consists of multiple formations that are not directly hydro-geochemically linked.
2. The groundwater source of seeps and springs located at the mouth of Unaweep Canyon originates from either of the likely aquifers.

In order to address the stated hypothesis, objectives for this study include collecting surface water, domestic well, seep, and spring samples to understand the aquifer systems present at Unaweep canyon. Another objective involves collection of these water samples in the spring, summer and fall to account for seasonality effects that can also be used to trace the origin of water in the canyon.

2. GEOLOGIC SETTING AND HYDROLOGY

2.1 Geology of Unaweep Canyon, Colorado

Unaweep Canyon (Mesa County, Colorado, U.S.A.) consists of massive exposed igneous and metamorphic Precambrian basement capped with Mesozoic sedimentary rocks (Soreghan et al., 2015) that contains the West Creek and East Creek Watersheds (Figure 1). Today, the canyon's outer steep walls are ~ 1km deep and 6 km wide, while its inner part is ~ 400m deep and 3km wide (Soreghan et al., 2009).

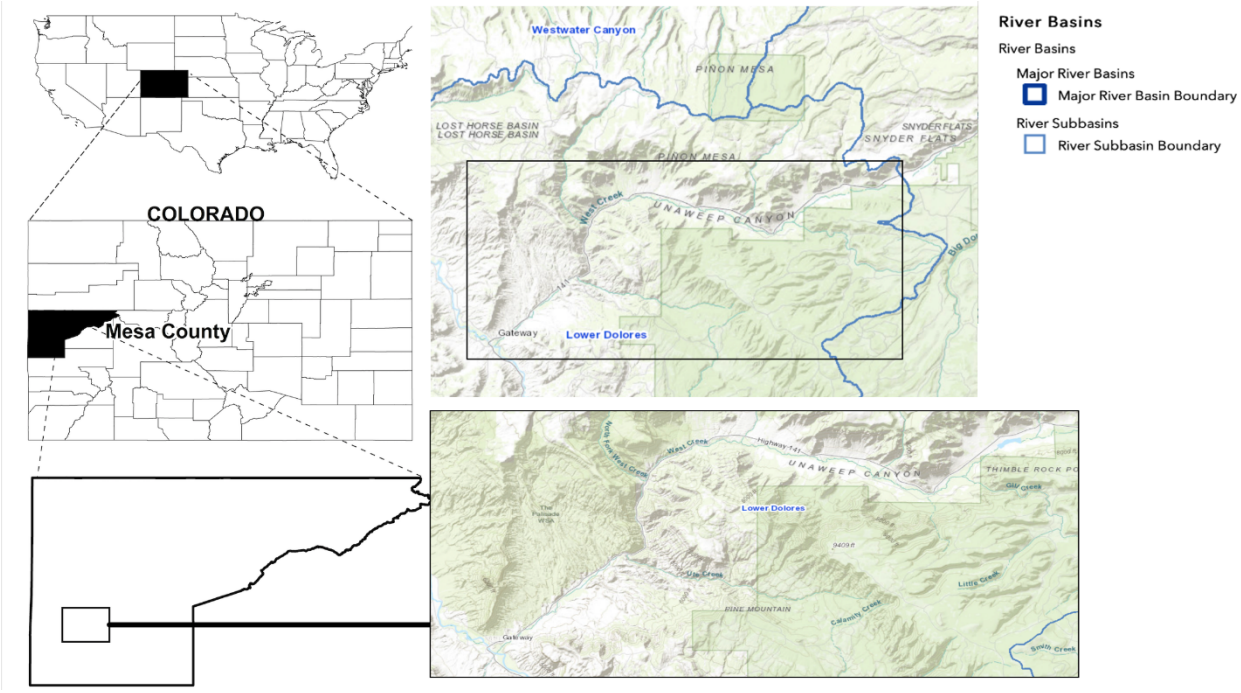

Figure 1. Location of the West Creek Watershed and Unaweep Canyon study site.

The processes surrounding the formation of Unaweep Canyon remains debated, with three possible hypotheses: 1) Fluvial incision in the late Cenozoic; 2) Glacial incision in the Pleistocene (late Cenozoic); and 3) Glacial incision in the late Paleozoic (late Carboniferous -Early Permian) followed by latest Paleozoic-Mesozoic burial and finally, partial fluvial exhumation of the buried valley by the Gunnison River (Hood, 2011, Marra, 2008, Soreghan et al., 2009, Soreghan et al., 2015). The third hypothesis has been supported by several studies (Soreghan et al., 2015) and forms the basis of this research as these processes set the stage for subsequent depositional events that led to the physical settings of the study site and associated aquifer system(s).

Unaweep Canyon is drained by East and West creeks that flow in opposite directions from the nearly imperceptible Unaweep Divide at an elevation of 2148m. East Creek joins the Gunnison River near Whitewater, Colorado, and West Creek flows into the Dolores River near Gateway, Colorado (Soreghan et al., 2015). At ~1.4 Ma, an inferred mass-wasting event at the western end

of the canyon resulted in the damming of the ancestral Colorado or Gunnison river, which led to the formation of a lake resulting in the deposition of lacustrine deposits (Balco et al., 2013, Marra, 2008). The lake eventually filled up with organic-rich sediments forming well defined lacustrine deposits, and the ancestral Gunnison River ultimately abandoned the canyon flowing eastward (Marra, 2008, Soreghan et al., 2009, Soreghan et al., 2015). Above the lacustrine unit is approximately 160 m of colluvium deposits, recording mass wasting of sidewall canyon debris with an approximate age of mid-late Pleistocene (ca. 0.9 Ma; (Marra, 2008, Balco et al., 2013, Soreghan et al., 2015)). Following the mass wasting, the alluvial aprons stabilized, marked by heavily vegetated surfaces and well developed Calcisols (Soreghan et al., 2015).

The type and sequence of deposits as described by the Pleistocene depositional history is evidenced in well log data from domestic wells (Fig. 2) in Unaweep Canyon as well as a generalized core log (Fig. 3) from a borehole that penetrated to a depth (below ground surface) of approximately 330 m (Soreghan et al., 2015). As recorded in this well penetration, the canyon fill includes three primary stratigraphic units above Precambrian basement: a basal unit (<15 m) of inferred upper Paleozoic strata, succeeded by Pleistocene lake and and mass wasting deposits, the latter two separated by an pedogenic interval (Marra, 2008, Soreghan et al., 2015). The lacustrine deposits comprise medium sand underlain by fine clayey sand with plant fragments. These lacustrine deposits document the presence of a lake bearing the same burial age as the lowest terraces of the Gateway (ancestral Gunnison River) gravels found close to the canyon's western mouth (Balco et al., 2013), effectively recording the near-abandonment age of the ancestral Gunnison River in Unaweep Canyon.

A.

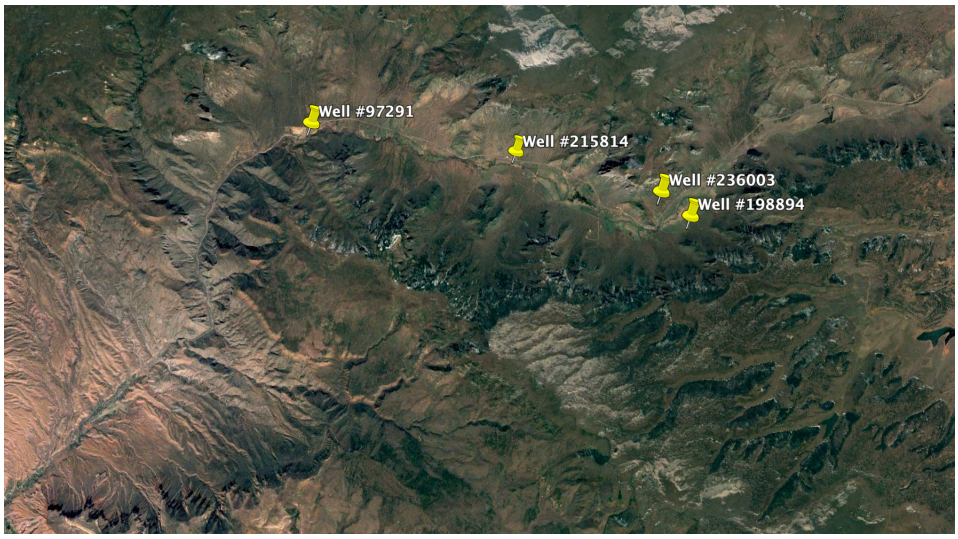

B.

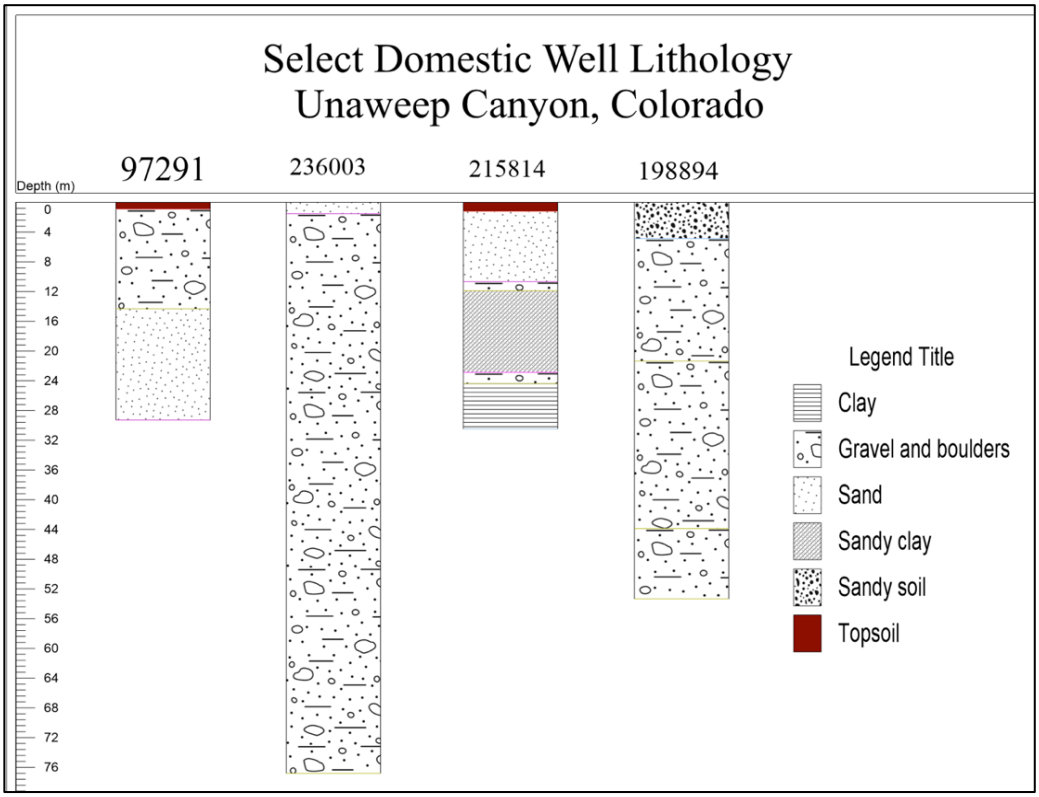

Figure 2. Map view and core profiles of lithological descriptions from domestic water wells installed in Unaweep Canyon. The well lithology information was obtained from well logs obtained from the Colorado Division of Water Resources (https://dwr.state.co.us/)). The numbers above each profile represent the well identification number recorded by the Colorado Division of Water Resources.

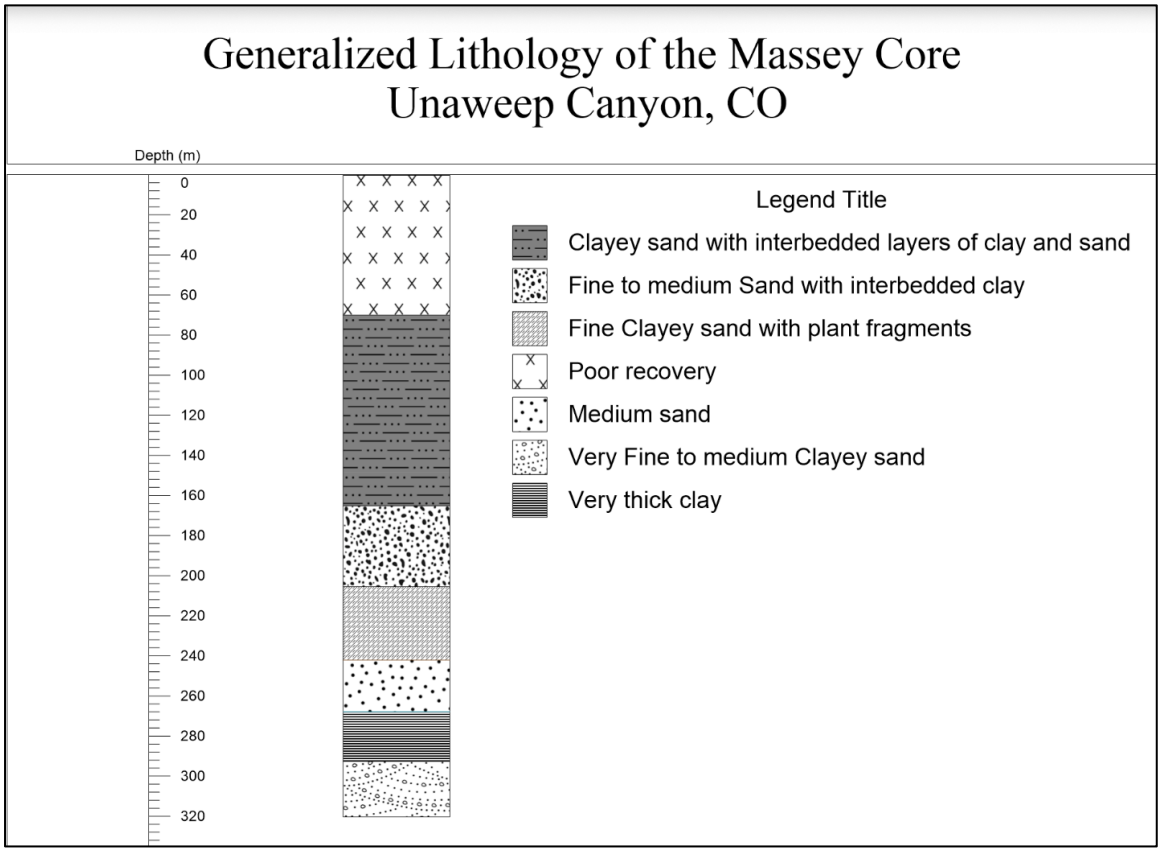

Figure 3. Generalized Massey Core log from Marra (2008). The core log was simplified by consolidating intervals that had similar lithology. Poor recovery includes brown coarse to fine sand cuttings with boulders up to 70m.

2.2 Hydrology of Unaweep Canyon

2.2.1 Climate

The study area is located in the West Creek watershed with an estimated drainage area of 177 km^2 that spans from the Unaweep Divide to the Dolores River at Gateway Colorado (Figure 4) (USGS StreamStats, 2016). The watershed has a maximum elevation of approximately 3000m from the upper reaches of the watershed to a minimum elevation of 1390 m near Gateway (USGS StreamStats, 2016). The region is semi-arid with a MAP of 50.72 cm, which falls mostly as snow in winter (USGS StreamStats, 2016), with minimal precipitation (other than afternoon storms) in

summer (Colorado State University, 2019). The temperatures range from 5.9 – 21.2°C in the summer and -5.9 – 11.4°C in the winter (Colorado State University, 2019).

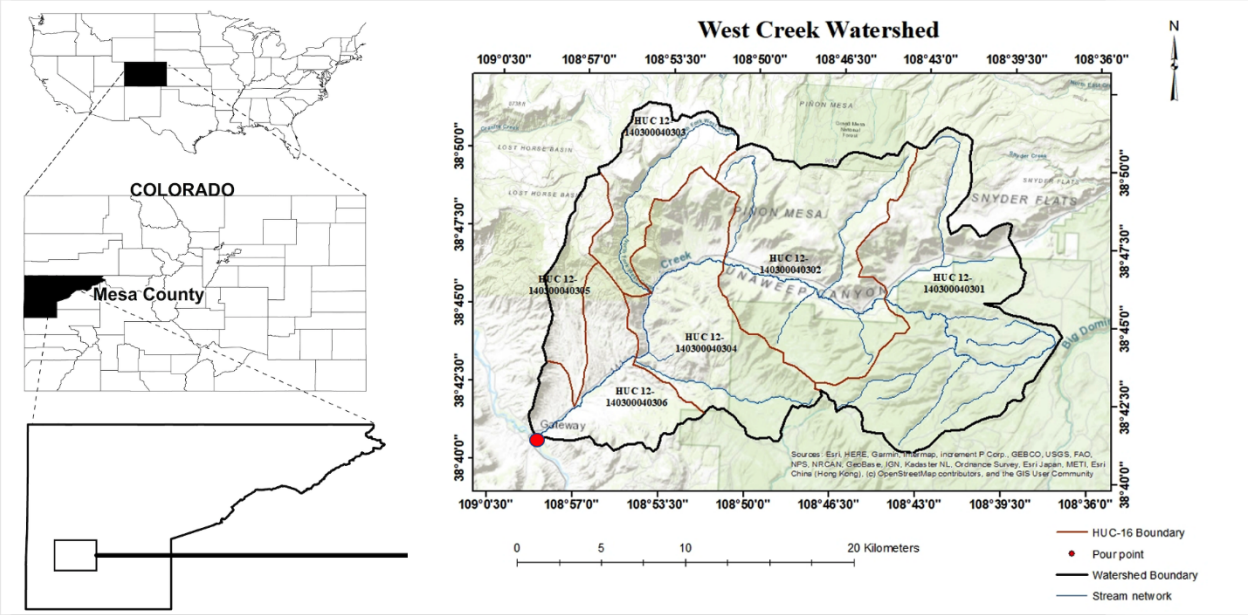

Figure 4. Map of the West Creek Watershed and associated Hydrologic Unit Code (HUC) boundaries. The West Creek stream network is also shown as well as the confluence of West Creek and the Dolores River (Red dot). Data was retrieved from USGS Streamstats (http://water.usgs.gov/osw/streamstats/colorado.html) and National Hydrography Dataset (https://www.usgs.gov/core-science-systems/ngp/national-hydrography/).

2.2.2 Surface Hydrology of the West Creek Watershed

West Creek is the primary surface water feature within the West Creek watershed that drains into the Dolores River and eventually the Colorado River. The tributaries of West Creek generally begin near the watershed boundary and join West Creek at the bottom of the Unaweep Canyon valley. Due to a lack of hydrologic studies and permanent gaging stations in the West Creek Watershed, records of stream flow do not exist. However, direct observation and communication with residents indicates that stream flow in West Creek is likely perennial, with inflow from both snowmelt and groundwater. A USGS gaging station (Station number: 09179450)

on the Dolores River above Gateway provides insight into likely seasonal streamflow influenced by snow melt, sporadic precipitation in the summer, and baseflow periods. As shown in Figure 5, stream flow in the Dolores River during 2019 was influenced by snowmelt inflow beginning around late- April and peaking in June followed by summer recession (July - October) into baseflow (USGS, 2016). The 2019 season was an exceptionally wet year whereas 2018 and 2020 were below average as highlighted in Figure 5, which resulted in significantly less flow in the Dolores River and a shorter snowmelt period (Fig. 6). From Figure 6, snow water equivalence (SWE) results from the Columbine SNOTEL station on the Uncompaghre Plateau indicates that the year 2018 was a very dry year, 2020 average, and 2019 in the 80th percentile for the maximum snow water equivalent line (NRCS, 2021).

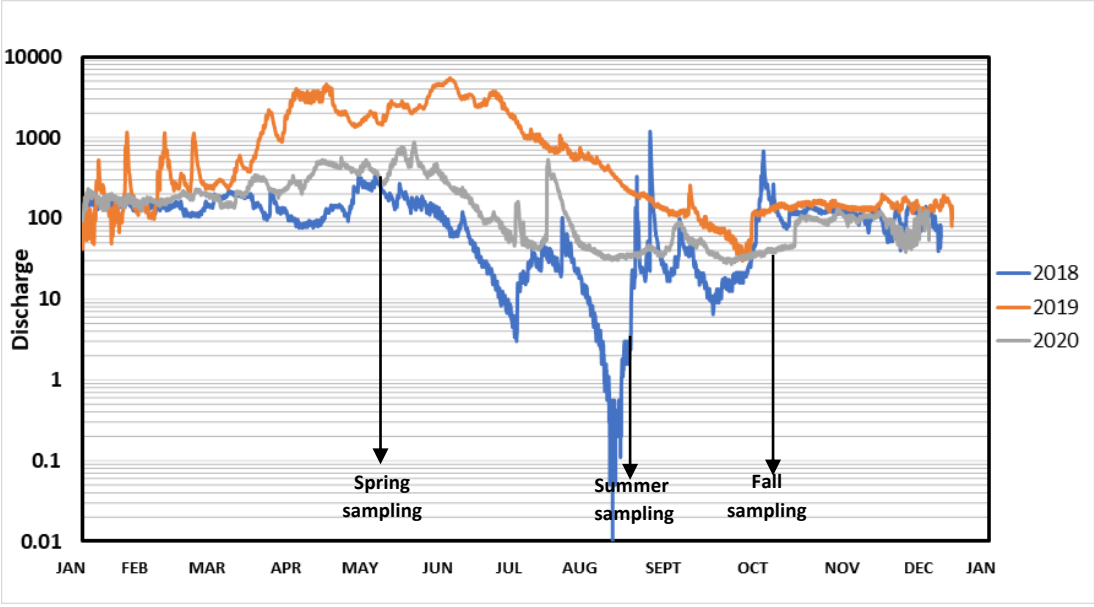

Figure 5. Modified Hydrograph from USGS stream gaging station (09179450) located near Gateway CO, for 2018, 2019 and 2020 (USGS, 2016). Note that stream discharge at the USGS gage station near Gateway is used as a proxy for periods of snowmelt, groundwater recharge, sporadic liquid precipitation, and baseflow owing to the lack of a gaging station in West Creek. Sampling dates for spring, summer, and fall 2020 are also shown.

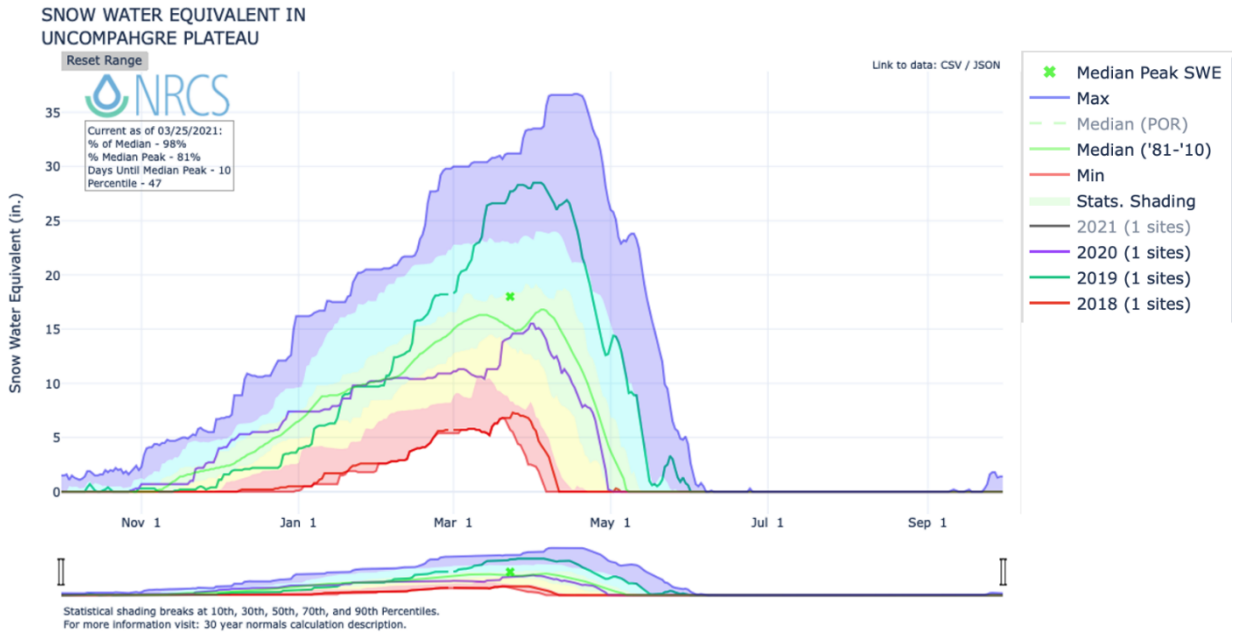

Figure 6. Snowpack conditions of Uncompaghre Plateau for the year 2018, 2019 and 2020 from the NRCS, which is used as a proxy to periods of snow accumulation due to the lack of a SNOTEL station in West Creek (NRCS, 2021; https://www.nrcs.usda.gov)

2.2.3 Groundwater in the West Creek Watershed

2.2.3.1 Shallow Groundwater

The nature and extent of groundwater in the study area is unknown. However, logs from domestic wells and the Massey Core (Fig. 2 and Fig. 3) indicate the presence of shallow groundwater in the region within the alluvial/colluvium deposits in the upper ~76 m. Behm et al. (2019) acquired seismic reflection data and inferred the presence of fanglomerate (alluvial deposits) in the western canyon, composed of ~160 m of clast- and matrix- supported conglomerate, with clasts of both the Mesozoic sand-siltstone and Precambrian basement. Pers. comm identified two interpreted aquifers (A1 and A2) based on previous electrical resistivity data (Fig. 7) which further confirms the presence of at least the shallow aquifer.

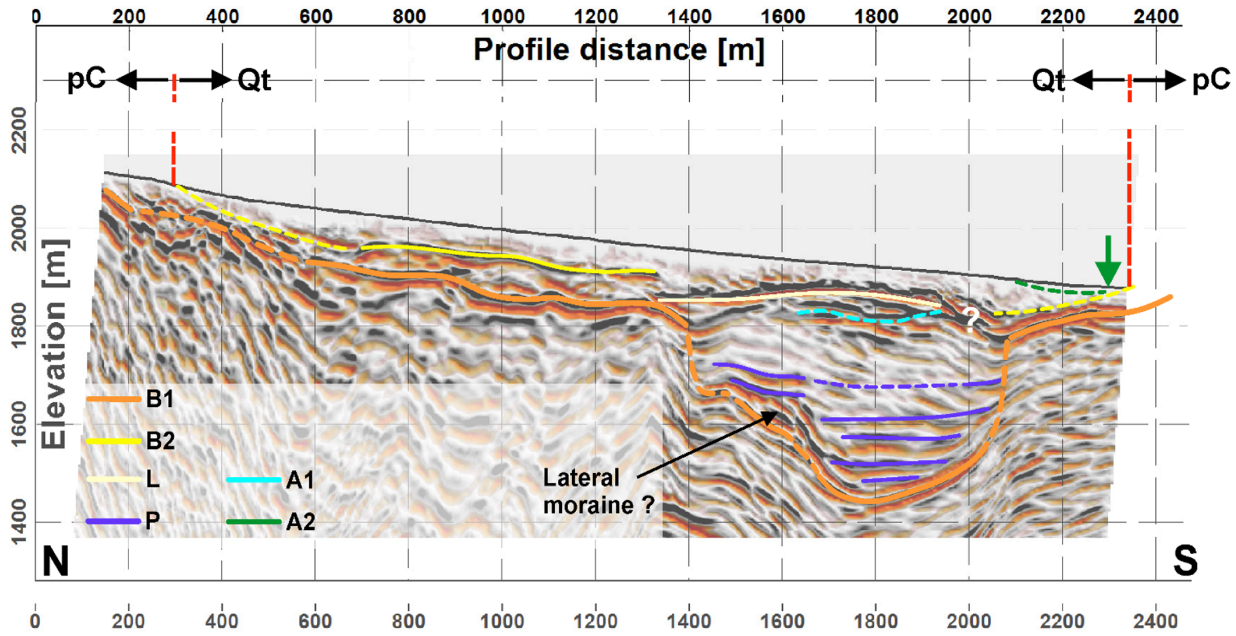

Figure 7. Integrated interpretation of the PSTM image, ground-truth data, and additional geophysical observable. Pc, Qt: Precambrian and quaternary surface cover. Dashed lines indicate where horizons are less well defined and/or are largely based on supplemental data. B1: Consolidated Precambrian basement. B2: Top of Precambrian regolith and pre-Quaternary sediments. L: Reflector associated with a Cenozoic lacustrine unit. P: pre-Quaternary sediments. A1, A2: Top of deep and shallow aquifers. (pers. comm).

2.2.3.2 Deep Groundwater

The nature and extent of deep groundwater in the West Creek watershed is unknown. However, a deeper confined aquifer is implied to exist from the description of lithology (Soreghan et al., 2015) where a confining clay-rich layer at a depth of 208 to 248 m lies above an aquifer with a composition that transitions from a medium clay-sand to medium sand with a total thickness of 24 m. Medium sand tends to exhibit a relatively high hydraulic conductivity ranging from 9×10^{-7} to 5×10^{-4} m/sec (Domenico and Schwartz, 1991), an average porosity between 29 – 49% and a specific yield of 32% (Morris and Johnson, 1966). Therefore, based on the likely intrinsic properties of high porosity and permeability typical of this type of aquifer material (Bjerg et al., 1992), the medium sand interval is potentially a deeper aquifer.

In Mesa County, there is a regional bedrock aquifer related to Precambrian basement rock fractures that store and transmit water (Colorado Geological Survey, 2017). A few domestic wells intercept fractured basement (Division of Water Resources, Colorado Support Decision Systems; (CDSS, 2017)). One of such well is well permit #155324 located in the study site and most of the other wells have been observed south and southwest of Colorado National Monument, where much faulting has occurred with the faulting decreasing towards the western county edge of the county (Colorado Geological Survey, 2017). These wells yield from 1-100 gallons per minute (Colorado Geological Survey, 2017).

However, despite the number of DWR permitted wells installed in Precambrian bedrock, no water quality data exist, other than a few results from springs, albeit none with sufficiently ion data to generate water-type pie charts (Colorado Geological Survey, 2017). The only data available were contamination data which showed that for the analyzed spring locations, primary maximum contaminant level (MCLs) was not surpassed, and the secondary maximum contaminant level (SMCLs) were only exceeded for TDS and sulfate at one spring (Colorado Geological Survey, 2017). At three springs, pH ranged between 7.6 and 8.2, within the acceptable SMCL range of 6.5 to 8.5 (Colorado Geological Survey, 2017). Therefore, this study aims to fill in the gap of providing sufficient data to be able to identify the water types present in the Precambrian bedrock.

2.2.3.3 Wetlands

Wetlands occupy approximately 1.5% of the total area of the West Creek Watershed (USGS StreamStats, 2016). These wetlands include the Unaweep Seep Natural area, a designated critical habitat (Doyle et al., 2002). The Unaweep Seep Natural area - a CNHP Potential Wetland Conversation Area- is home to Unaweep Seep, one of the seeps in the area (Fig. 6). A combination of wet meadows, marsh, sedge, cottonwood, willows and more and a rare assembly of plants

including the Joe-pye weed, panic manna grass and giant helleborine orchid have been documented in the Unaweep Seep Natural area (National Audubon Society, 2020). A 1983-84 survey of the area revealed it as the richest landbird site in west-central Colorado (National Audubon Society, 2020). Since springs and seeps are locations where groundwater saturates the surface, the water for the springs and seeps in the West Creek watershed likely originates from groundwater, and based on field observation, these wetlands occur wherever these seeps/springs exist.

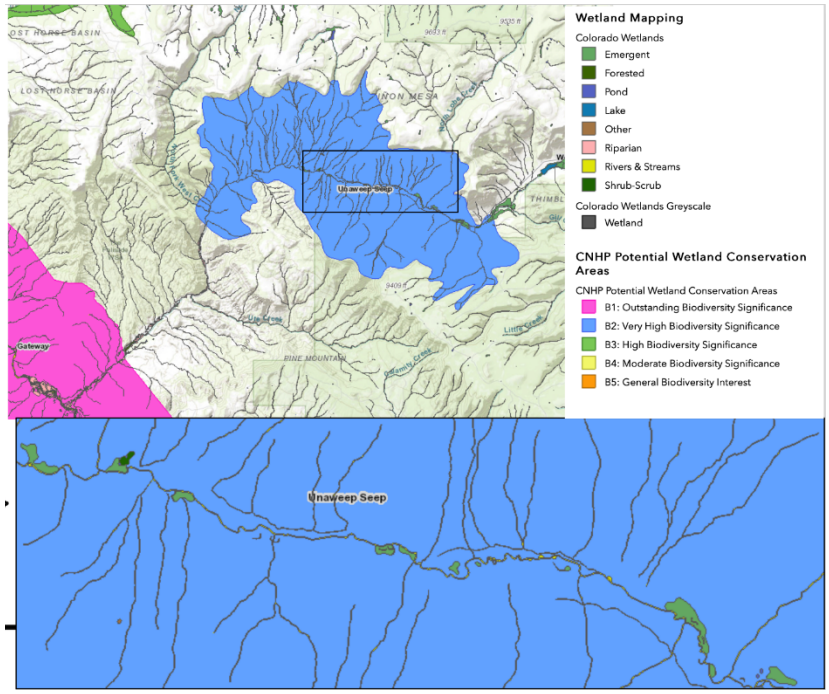

Figure 8. Map indicating locations and degree of wetland sensitivity in Unaweep Canyon. Unaweep Seep is indicated including areas of significant wetland biodiversity. Unaweep Canyon has been identified as a CNHP Potential Wetland Conversation Area with a Very High Biodiversity significance (https://www.arcgis.com/apps/webappviewer/index.html?id=a8e43760cb934a5084e89e46922580cc).

3. MATERIALS AND METHODS

3.1 Sampling and In-Situ Water Chemistry

Water samples from 3 seeps, 2 Precambrian bedrock springs, 2 domestic wells, and 3 surface water locations (West Creek) were collected during the spring, summer, and fall in 2020

(Fig. 9). Samples were collected once in-situ measurements of pH, temperature, conductivity, and total dissolved solids (TDS) stabilized (±10% between three consecutive measurements). A pre-calibrated HANNA™ HI 9829 multi-parameter probe was used for in-situ measurements of pH, Dissolved Oxygen (D.O.), Specific conductivity (SpC), temperature (°C), Oxidation-Reduction Potential (O.R.P.), and Total Dissolved Solids (T.D.S.). The probe was calibrated using pH buffer solutions (Orion Application Solutions) of 4.01 (Orion 910104), 7.00 (Orion 910107), and 10.01 (Orion 910110).

Table 1. Sampling Locations with coordinates and brief descriptions regarding source or distinct features.

Site ID	**Coordinates**		**Brief Description**
	Latitude	**Longitude**	
UNA-18-1	38°46'37"N	108°50'32"W	Organic rich seep located on the Moore property. Seep appears to be an excavated depression. Sample was collected close to where seep emerges from the surface.
UNA-18-4	38°46'15"N	108°53'21"W	Base of Unaweep seep near overpass. High organic content, heavily vegetated/grassy. Inaccessible in the summer sampling event due to vegetation overgrowth
UNA-18-14	38°46'36.24"N	108°51'1.76"W	Seep coming out of hillside, located west of Moore's house on the Moore's property. High organics, well vegetated
UNA18-2 June	38°46''33"N	108°50'25"W	West Creek on Moore property, across UNA-18-1.

UNA18-7 June	38°46’17”N	108°53’11”W	West Creek across from Unaweep Seep, located below the bridge before the picnic area.
UNA18-10 June	38°44’0”N	108°54’10”W	West Creek at Picnic area. Creek is across the street from the Old mine adit (UNA18-12)
UNA18-11 June	38°43’58.02”N	108°54’6.23”W	Old mine adit (seep) in Precambrian basement. Sample collected from seepage on roadside bank
UNA18-12-1 June	38°43’28”N	108°54’58”W	Smells of sulfur, salt precipitate. Spring is known as the Wright Spring from the Mesa County report. Looks like an old adit, developed in the Precambrian basement located on a hillside approximately one mile from the road
UNA-19- June	38°46’35”N	108°50’47”W	Well depth of 96ft. Owners are the Moores.
UNA-20- June	38°46’12”N	108°48’8”W	Well depth of 140ft, DTW: 70ft (information from owners). Owners are Amy and Fred Bolton

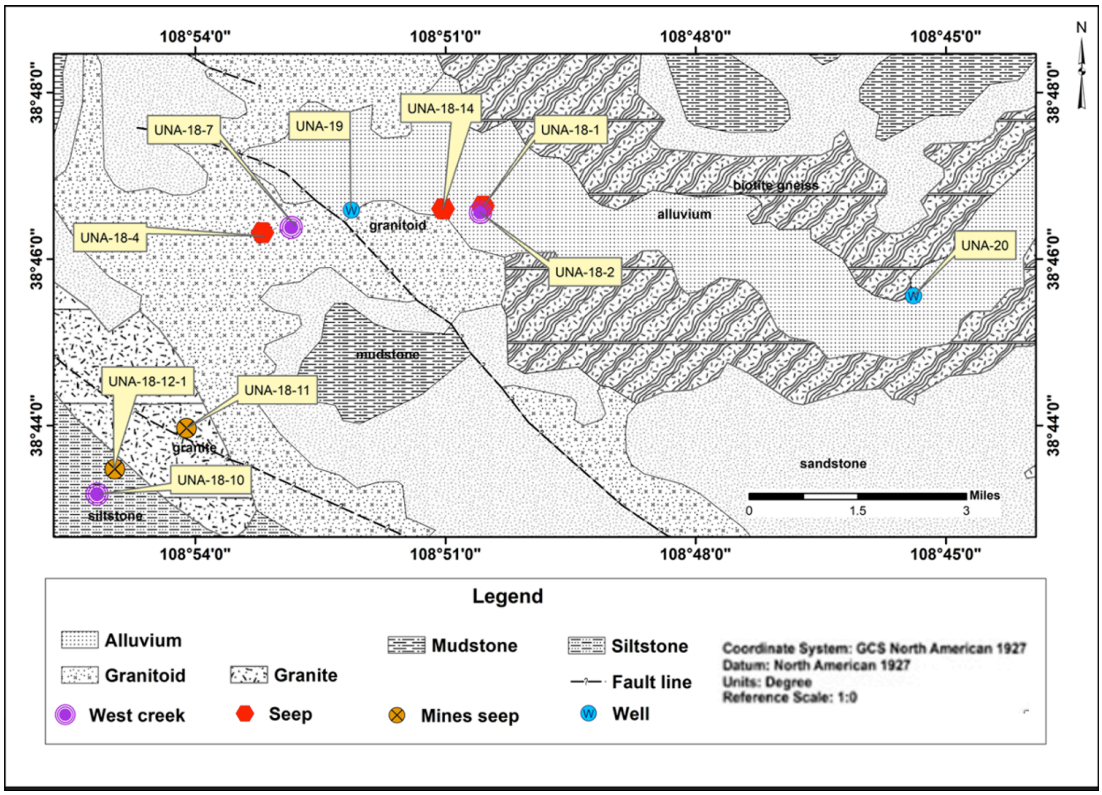

Figure 9. Map of sampling locations separated by their type. The geologic map of the area is shown to indicate subsurface lithology and structures in relation to sample points.

3.2 Laboratory Analysis

3.2.1 Major Anions

Samples for major anions were filtered (0.45 µm nominal pore size) into pre-cleaned (acid-washed and rinsed with nanopure water) 60 mL HDPE bottles and stored at 4°C until analysis. Anion analysis was completed by Ion Chromatography (Dionex ICS-1100) in the Aqwatec Laboratory (Colorado School of Mines, Golden, CO). Anions measured by IC included fluoride (F^-), bromide (Br^-), nitrite (NO_2^-), chloride (Cl^-), phosphate (PO_4^{3-}), sulfate (SO_4^{2-}), and nitrate (NO_3^-) ions. Quality assurance and quality control (QA/QC) included analysis of laboratory blanks and calibration checks after every tenth primary sample including the beginning and end of each run. The laboratory blanks consisted of deionized, ultrapure water for which readings below the

instrument detection limit are satisfactory. Calibration checks consisted of a low and high range sample with known concentrations analyzed once per group of 10 primary samples and at the beginning and end of each analytical run. The calibration check results are considered valid and acceptable if the measurements were within ±10% of known concentration. If anion results exceeded the calibration dynamic range, the samples were diluted and rerun to ensure accuracy.

3.2.2 Metals

Metal samples included collecting only the dissolved fraction at each site since this study focused on the solute phase. Water samples were filtered through a Titan3™ PVDF 0.45µm syringe filter attached to a polypropylene Fisherbrand™ 60 mL sterile syringe into 60 mL HDPE bottles. Major cations included Ca, Mg, Na, and K, and trace metals included Al, As, B, Ba, Cd, Cu, Cr, Fe, Li, Mn, Mo, Ni, Pb, Se, Si, Sr, Ti, Tl, U, V, and Zn.

Metals samples were preserved with approximately 0.5 mL 70% trace metal grade nitric acid and stored at 4°C until analysis. The metal analysis was completed by a PerkinElmer 8000DV Inductively Coupled Plasma Optical Emission Spectroscopy (ICP-OES) at the Colorado School of Mines (Golden, CO) Atomic Spectroscopy Laboratory. Quality assurance and quality control (QA/QC) included the analysis of laboratory blanks, calibration checks, NIST certified standard reference material (SRM), and an internal standard. The laboratory blanks consisted of deionized, ultrapure water for which readings below the instrument detection limit (BDL) were satisfactory. A multi-element continuing calibration verification (CCV) solution was measured at the beginning, end, and after every tenth primary sample to ensure the validity of the instrument calibration throughout the analysis. Acceptable CCV values are within ±20% of the known concentrations. The NIST 1643f SRM (https://www-s.nist.gov/srmors/view_detail.cfm?srm=1643F) was analyzed at a frequency of once per group of

30 primary samples for which measured values that are ±10% of the certified concentrations are deemed acceptable. Scandium (Sc) was included as an internal standard added to each aliquot (calibration, blank, SRM, CCV, and primary solutions) measured in each analytical run to account for instrument drift and potential salt deposition within the sample introduction system. Acceptable Sc concentrations were within 20% of the known concentration (1mg/L ±0.2mg/L).

3.2.3 Alkalinity

Alkalinity was measured on-site using a Hach™ digital titrator (Hach™ Method 8203 Phenolphthalein and Total Alkalinity) to minimalize potential variability associated with changes in water temperature and pH. Measured alkalinity (as mg/L $CaCO_3$) results were then evaluated by Visual MINTEQ (https://vminteq.lwr.kth.se/download/) to estimate the concentrations of bicarbonate (HCO_3^-) and carbonate (CO_3^{2-}) components necessary for Piper diagrams.

3.2.4 Stable Oxygen and Hydrogen Isotopes

Isotope samples were collected by filtering site water through a Titan3™ PVDF 0.45µm syringe filter syringe filter attached to a polypropylene Fisherbrand™ 60 mL sterile syringe into borosilicate 30ml glass vials with Polyseal caps. Special care was taken to avoid any headspace in each sample by filling each vial to where a visible meniscus forms at the top prior to capping to prevent any sampling error related to fractionation of the isotopes. Isotope analysis focused on ^{18}O and ^{2}H necessary for comparison with the global meteoric water line (GMWL). Due to instrument difficulties at the University of Georgia's Center for Applied Isotope Studies (CAIS) laboratory isotope samples collected during the Summer and Fall were measured at the UC Santa Cruz Stable Isotope Laboratory.

At CAIS, the stable isotopic oxygen and hydrogen compositions of water were measured using the Cavity Ring-Down Spectroscopy (CRDS) technique. A Quality assurance and quality control (QA/QC) included performing each measurement 7 times and using the last 3 results for further calculation to minimize potential memory effect. The standards used to calibrate the measured data include the IAEA reference waters (VSMOW2, GISP, and SLAP2), and the calibrated $\delta^{18}O$ and $\delta^{2}H$ values are reported relative to VSMOW. The precision for analyzing water samples with natural abundance are usually ≤ 0.20 ‰ for $\delta^{18}O$ values and ≤ 1.0 ‰ for $\delta^{2}H$ values based on the internal database at CAIS.

At the UC Santa Cruz Stable Isotope Laboratory, a Picarro L2130-i isotope analyzer was used for stable isotope analysis. The isotope ratio measurements of samples were corrected to VSMOW against measurements of the international standard reference materials SMOW, GISP, and SLAP. The reproducibility of duplicates was 0.02 ‰ for $\delta^{18}O$ and 0.08 ‰ $\delta^{2}H$.

3.2.5 Dissolved Organic Carbon (DOC)

DOC samples were collected by filtering (0.45 µm nominal pore size filter) site water into pre-combusted, pre-cleaned 30 ml glass amber sample bottles and stored at 4ºC until analysis. DOC analysis was performed using high-temperature combustion with NDIR detection (Shimadzu™ TOC-L) in the Aqueous Geochemistry Laboratory (AGL) at the University of Oklahoma. The AGL uses a non-purgeable organic carbon (NPOC) method for DOC analysis that negates potential interferences caused by inorganic carbon. The NPOC method has an estimated MDL of 20 to 30 µg C/L, which was sufficient for the low DOC concentrations (<1.0 mg C/L) measured in the samples collected in this study. QC checks included the use of blanks and calibration check standards. Blanks consisted of deionized, UV-treated water measured throughout

each analytical run. Calibration check standards consisted of aliquots with DOC concentrations of 3 mg C/L and 5 mg C/L as potassium hydrogen phthalate (KHP).

3.2.6 Rare Earth Elements (REE)

The same metal samples were also analyzed for REEs. The REE analysis was done using the prepFAST IC autosampler attached to a PerkinElmer NexION2000 Inductively Coupled Plasma (ICP)-MS which was tuned using a standard daily tuning solution by TUNE B iCAP THERMO TS with a matrix of 2.5% v/v nitric acid / 0.5% v/v hydrochloric acid. Calibration used the following elements: cerium (Ce), dysprosium (Dy), erbium (Er), europium (Eu), gadolinium (Gd), holmium (Ho), lanthanum (La), lutetium (Lu), neodymium (Nd), praseodymium (Pr), Samarium (Sm), Terbium (Tb), Thorium (Th), Thulium (Tm), uranium (U), ytterbium (Yb), and yttrium (Y) at concentrations of 0.1, 0.5, 1, 5, and 10 ppb in 2% nitric acid. Prior to analysis all groundwater samples were diluted 10-fold into 2% ACS reagent grade to obtain a final volume of 5mL to keep the measured concentrations within the dynamic range of the calibration curve. An internal standard consisting of 5ppb of Iridium (Ir) was used throughout the entire analysis.

4. RESULTS

4.1. Water chemistry

4.1.1 In-situ water chemistry

Table 2 shows select in-situ water chemistry results, and Appendix 1 lists comprehensive in-situ results. These in-situ parameters were selected because they showed the most variation among sites, possibly related to different hydrologic processes. Generally, the West Creek (surface water) sites (UNA-18-2, UNA-18-7 and UNA-18-10) exhibit slightly higher pH values than all

other sites, whereas the Precambrian bedrock spring samples (UNA-18-11 and UNA-18-12-1) exhibit higher temperature and conductivity values (Table 2, Fig. 10). Alkalinity (Figure 10C) is greater in the seeps, West Creek, and the domestic wells relative to the Precambrian bedrock spring samples. The pH (Figure 10E) for the surface water ranges from 7.5 to 8.56, the seeps 6.78 to 8.18, the domestic wells 6.84 to 7.29 and the Precambrian bedrock spring 6.99 to 7.74. The largest variation in the in-situ water chemistry data were the conductivity values (Table 2) measured in the Precambrian bedrock spring samples relative to other sites. The conductivity and TDS values generally ranged from 317 to 436 µS/cm for the West Creek, seeps, and domestic well samples for all the seasons. However, for the Precambrian bedrock spring samples, the conductivity and TDS values were approximately one order-of-magnitude greater than the other sites with values that ranged from 2422 to 2788 µS/cm, likely reflecting greater residence time along groundwater flowpaths.

Table 2. In-situ results for the sampling sites included in this study. Sample dates are included to show results for spring (6/6/20), summer (8/17/20), and fall (9/14/18 and 10/6/20) seasons. Complete tabulated in-situ water chemistry results are found in Appendix 1.

Sites	**Sample Date**	**pH**	**Temp.**	**ORP**	**Alkalinity**	**Conductivity**
		S.U.	°C	mV	mg/L as $CaCO_3$	µS/cm
UNA-18-1	9/14/18	7.46	11.9	196	182	319
UNA-18-1	6/6/20	7.65	11.9	193	240	389
UNA-18-1	8/17/20	7.50	12.1	197	197	428
UNA-18-1	10/6/20	7.36	11.6	192	225	433
UNA-18-2	9/14/18	7.98	13.2	194	42	293
UNA-18-2	6/6/20	8.14	19.6	183	202	402
UNA-18-2	8/17/20	7.98	19.6	187	233	386
UNA-18-2	10/6/20	7.50	11.6	196	231	416
UNA-18-4	9/15/18	8.18	12.9	195	38	362
UNA-18-4	6/6/20	7.99	16.7	185	163	377
UNA-18-4	10/6/20	7.99	15.6	188	210	368
UNA-18-7	9/14/18	8.53	16.3	194	68	331
UNA-18-7	6/6/20	8.60	16.6	183	175	375
UNA-18-7	8/17/20	8.51	17.5	188	184	345
UNA-18-7	10/6/20	8.28	8.7	195	232	376

UNA-18-10	9/14/18	8.56	18.7	187	53	277
UNA-18-10	6/6/20	8.47	16.9	182	118	317
UNA-18-10	8/17/20	8.43	15.8	196	167	360
UNA-18-10	10/6/20	8.28	9.7	191	204	368
UNA-18-11	9/14/18	7.66	20.2	199	33	2506
UNA-18-11	6/7/20	7.02	15.2	197	31	2788
UNA-18-11	8/17/20	7.02	21.0	195	69	2512
UNA-18-11	10/6/20	6.99	14.5	196	41	2422
UNA-18-12-1	9/14/18	7.74	20.5	189	57	1353
UNA-18-12-1	6/7/20	7.67	19.6	177	115	1563
UNA-18-12-1	8/17/20	7.63	21.6	185	50	1579
UNA-18-12-1	10/6/20	7.44	20.2	185	57	1573
UNA-18-14	9/15/18	7.29	12.9	194	71	339
UNA-18-14	6/6/20	6.98	11.3	189	266	426
UNA-18-14	8/17/20	7.06	11.6	198	234	408
UNA-18-14	10/6/20	6.78	13.9	188	266	217
UNA 19	6/6/20	7.29	11.1	192	210	324
UNA 19	8/17/20	7.19	17.1	191	202	339
UNA 19	10/6/20	6.95	13.1	194	205	346
UNA 20	6/6/20	7.01	12.4	190	199	425

UNA 20	8/17/20	7.00	12.6	195	181	410
UNA 20	10/6/20	6.84	12	194	230	410

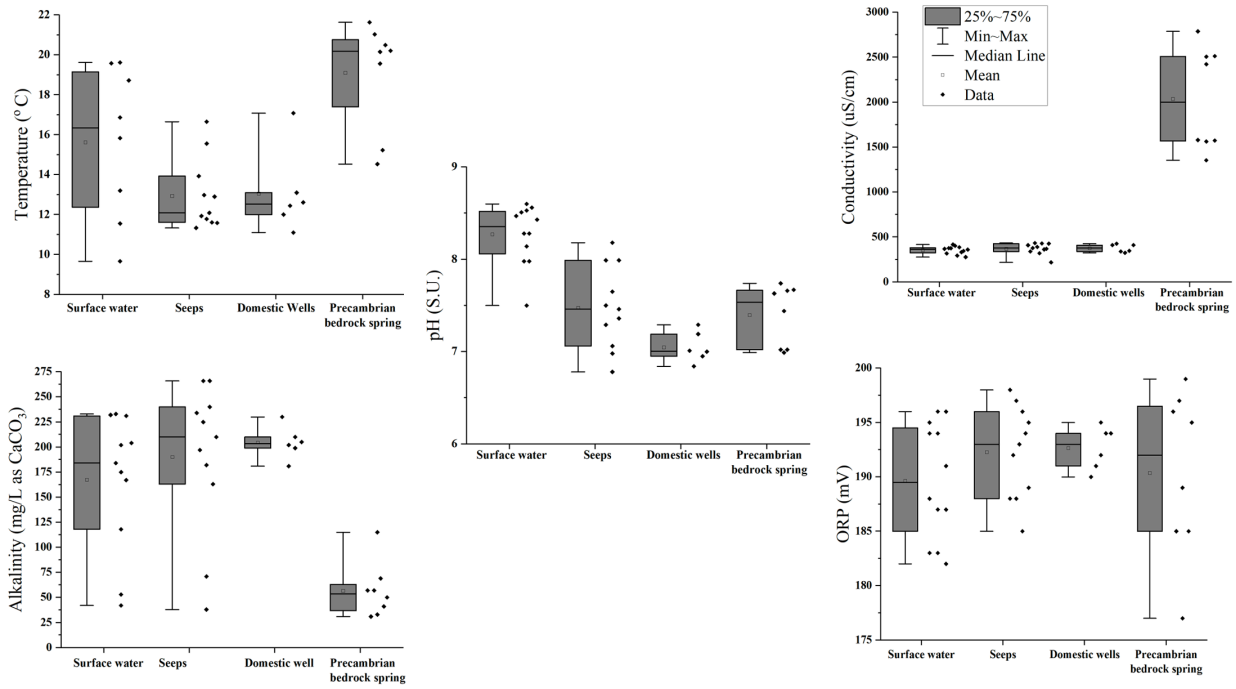

Figure 10. Box plots for temperature (A), conductivity (B), alkalinity (C), ORP (D), and pH (E) by site type. The boxes encompass the 25% to 75% percentile among the data along with the median and mean values. Whiskers indicate the maximum and minimum values. Individual data points are shown to the right of each box to show any variance among data.

4.1.2 Metal and Anion data

Metal and anion results from all samples collected in 2018 and 2020 are shown in Figures 11A – 11D and Figures 12A – 12B. Appendix A shows comprehensive metal and anion results. The results selected show the largest differences among all sites and thus reflect various hydrologic processes. Figures 11 & 12 show that metal and anion concentrations in the Precambrian bedrock spring samples (UNA-18-11 and UNA-18-12-1) are generally larger than in the other sites. The U (Figure 11A) concentration is considerably greater in the streams and shallow groundwater than the Precambrian basement sites. Among the two Precambrian bedrock samples, Precambrian bedrock spring 1 (UNA-18-11) exhibits larger metal and anion concentrations than Precambrian bedrock spring 2 (UNA-18-12-1), possibly indicating different groundwater sources or flow pathways.

Piper plots (Figure 13) were created to evaluate hydrogeochemical diversity using major ion data (Mg^{2+}, Ca^{2+}, Na^{+}, K^{+}, SO^{2-}_{4}, Cl^{-} and CO^{2-}_{3}+HCO^{-}_{3}) from all sites sampled in 2018 and 2020. Appendix 4 shows Piper plots with individual sampling events by year and season. The Piper plot suggest three distinct water types amongst all the samples (Fig. 13). The seeps, West Creek and domestic wells all cluster together around the Mg–HCO^{-}_{3} water type while the Precambrian spring samples are of mixed and Ca-Cl water types. However, some of the West Creek and seep samples trend towards the Mixed type possibly due to mixing it interacting with the Mixed-type water. Seasonality induced by snowmelt and rain recharge is not very pronounced, likely attributable to persistent drought conditions in 2018 and 2020.

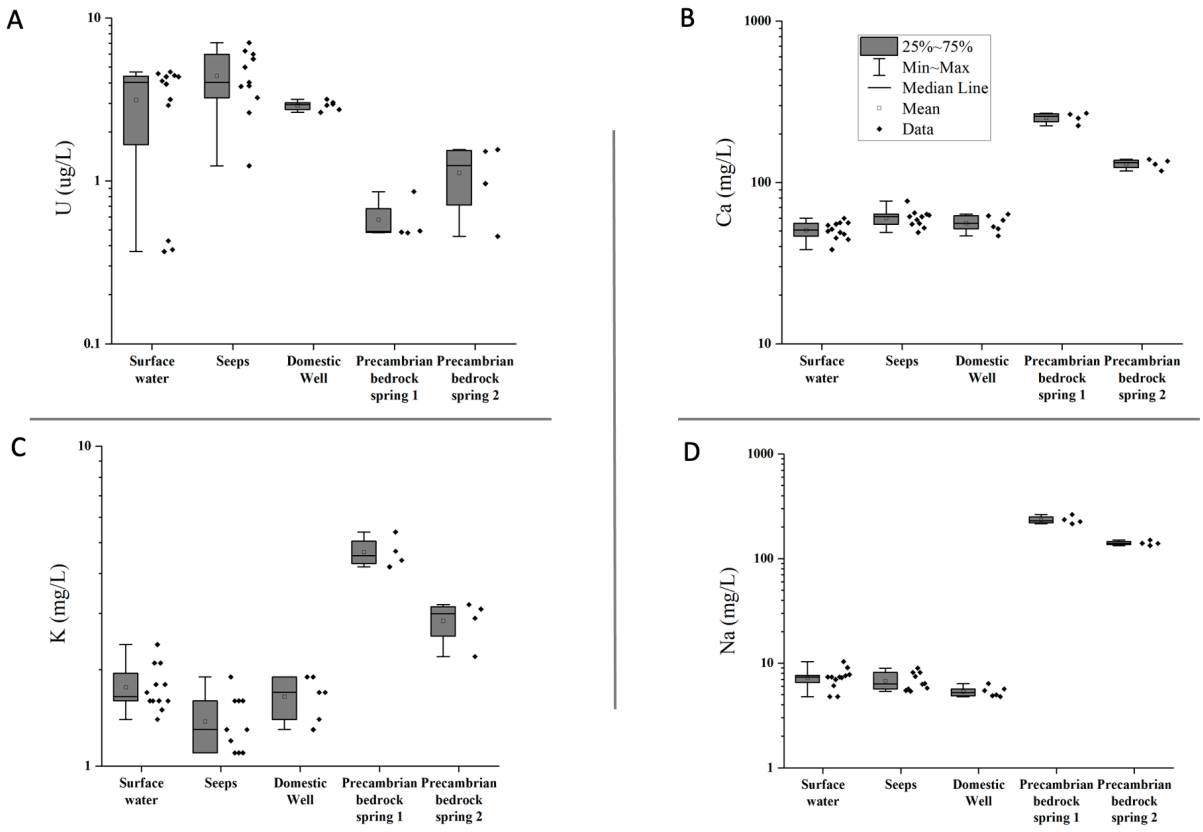

Figure 11. Box plots of metal results by site type. Individual data points to the right of each box show the variance. The boxes encompass the 25% to 75% percentile among the data along with the median and mean values. Whiskers indicate the maximum and minimum values. All plots used a log scale for the concentration values due to the orders of magnitude differences in concentration that exist among the sample sites. The Precambrian bedrock spring 1 represents UNA-18-11 while Precambrian bedrock spring 2 represents UNA-18-12-1.

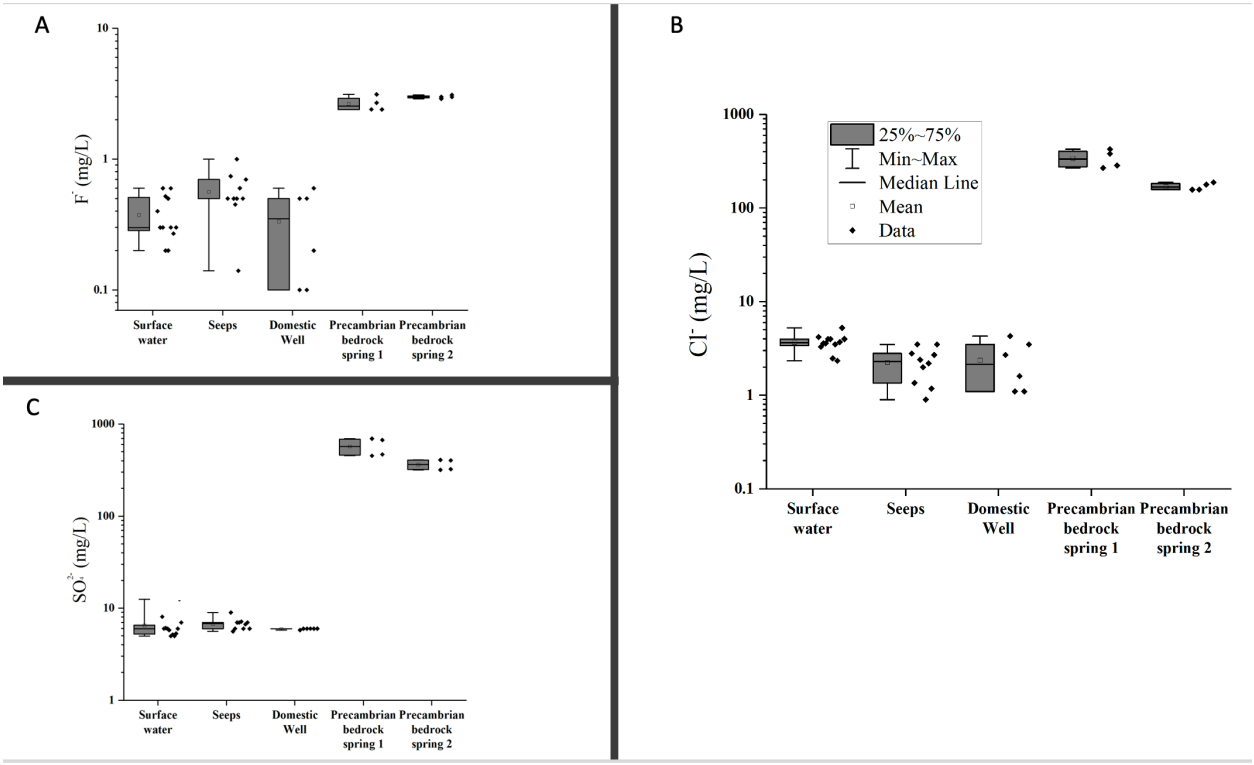

Figure 12. Box plots of anion results by site type. Individual data points to the right of each box show the variance. The boxes encompass the 25% to 75% percentile among the data along with the median and mean values. Whiskers indicate the maximum and minimum values. All plots used a log scale for the concentration values due to the orders of magnitude differences in concentration that exist among the sample sites. The Precambrian bedrock spring 1 represents UNA-18-11 while Precambrian bedrock spring 2 represents UNA-18-12-1.

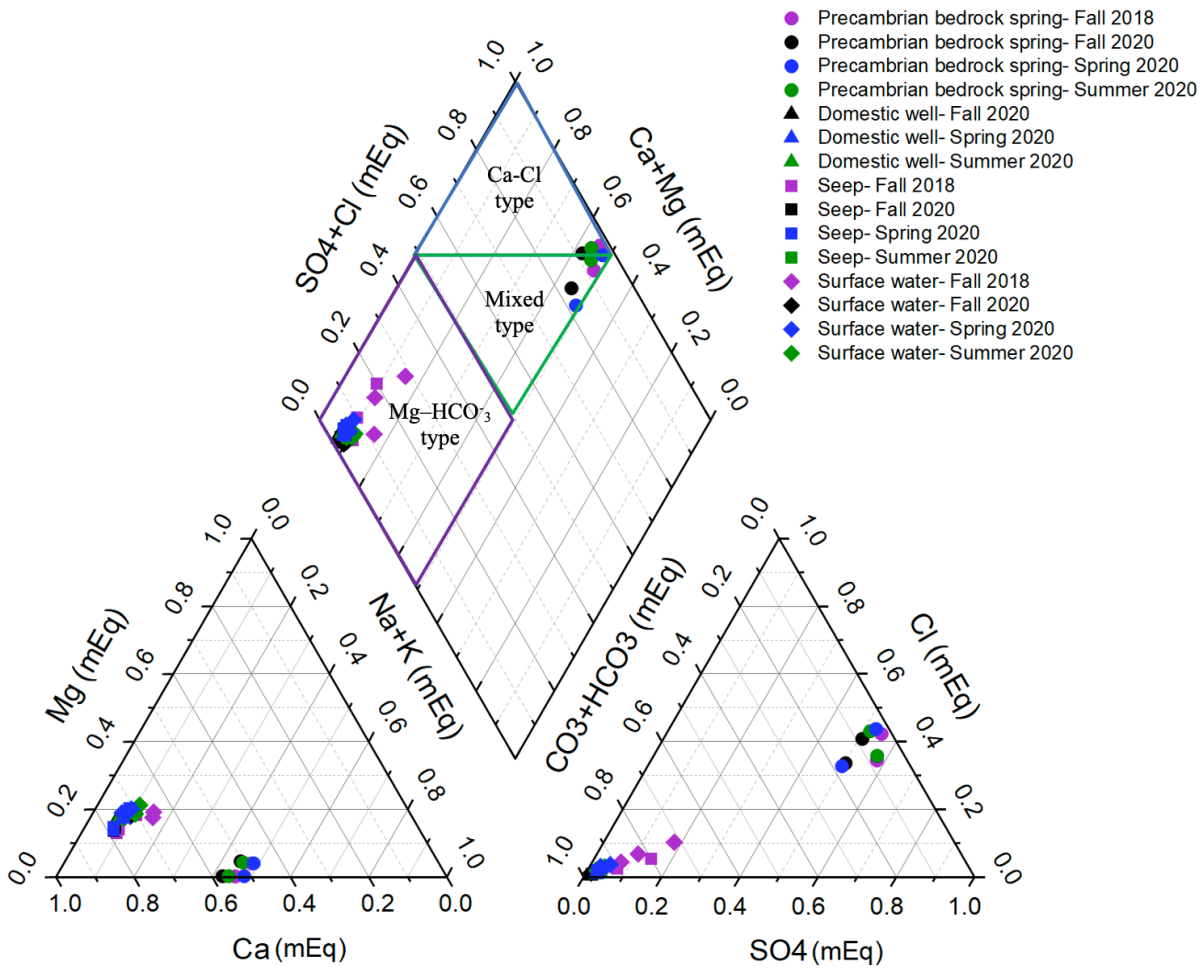

Figure 13. Piper plots representing major ion chemistry of all surface water and groundwater sampled in Unaweep Canyon in 2018 and 2020. Water type regions shown are from Piper (1944).

4.1.3 Rare Earth Elements (REE)

Appendix A shows comprehensive REE concentrations (in ug/L). Figures 14A – 14B show subsets of REE data to specifically illustrate differences between LREEs and HREEs in order to discern possible REE enrichment/depletion patterns. These REEs were selected because they showed the most distinct variation in concentrations and also studies (Johannesson et al., 1997, Duvert et al., 2015) indicate their usefulness in differentiating bedrock groundwater from other

water sources. Non-detect values were assigned a value of 0.001ug/L to ensure complete representation of all sites.

REE concentrations vary considerably between West Creek and groundwater where the concentrations of LREEs (^{89}Y, ^{139}La, ^{140}Ce and ^{142}Nd) are generally greater than what is found in groundwater (both shallow and deep), likely owing to fractionation with organic matter and possibly complexation with bicarbonate ions. Little variation occurs in REE concentrations in groundwater from the Precambrian bedrock springs and the shallow groundwater seeps. Possible seasonality was observed only for West Creek (surface water) where elevated concentrations of LREEs represent samples collected in the spring.

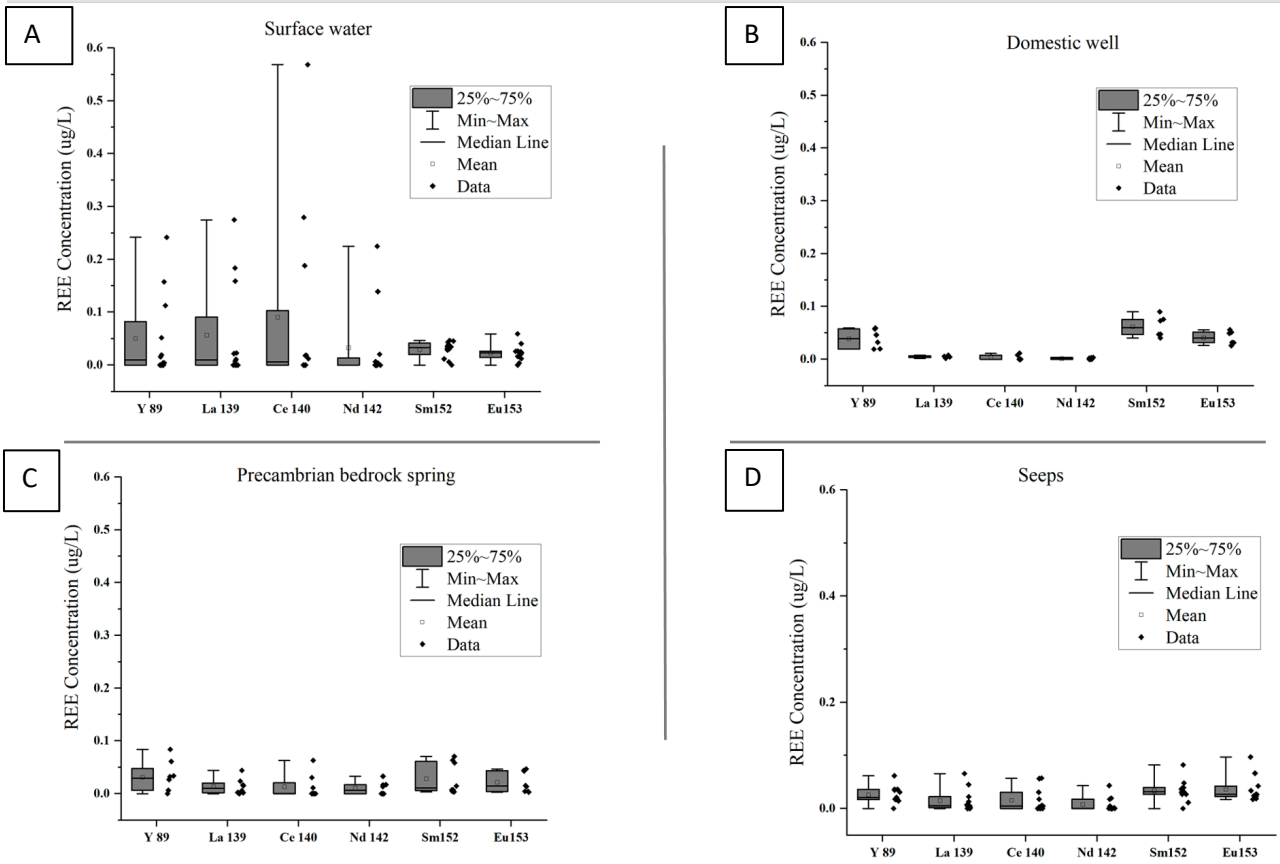

Figure 14. Box plots of REE concentrations of the different water samples as well as for the different sampling events, including September 2018. The boxes encompass the 25% to 75% percentile among the data along with the median and mean values. Whiskers indicate the maximum and minimum values.

4.2. ^{18}O and ^{2}H isotope composition

The isotopic data are reported in standard delta notation in parts per thousand relative to Vienna Standard Mean Ocean Water (VSMOW; (Coplen, 1994)). The isotopic data are plotted against the GMWL (Global Meteoric Water Line), $\delta^2H = 8\delta^{18}O + 10$, developed by Craig (1961). The GMWL is an average of various local meteoric water lines (LMWLs) controlled by local climatic factors, such as the origin of the vapor mass, as well as re-evaporation that occurs during rainfall and the seasonality of precipitation (Clark and Fritz, 1997). The isotopic composition of the seeps, West Creek, domestic well and Precambrian bedrock samples (Table 3) range from -

14.06 to -15.16‰ $\delta^{18}O$ and -103.5 to -109.46‰ $\delta^{2}H$, -12.89‰ to -14.7‰ $\delta^{18}O$ and -99.3 to -106.68‰ $\delta^{2}H$, -13.64 to -14.77‰ $\delta^{18}O$ and -102.4 to -105.94‰ $\delta^{2}H$, -14.27 to -15.39‰ $\delta^{18}O$ and -108.7 to -112.78‰ $\delta^{2}H$ respectively.

Table 3. $\delta^{18}O$ and $\delta^{2}H$ results from 2020.

Sample ID	**Sample Date**	**$\delta^{18}O$**	**$\delta^{2}H$**
		‰	‰
UNA-18-1	6/6/20	-14.3	-104.5
UNA-18-1	10/6/20	-14.8	-106.1
UNA-18-4	6/6/20	-14.6	-107.7
UNA-18-4	10/6/20	-15.2	-109.5
UNA-18-14	6/6/20	-14.1	-103.5
UNA-18-14	8/17/20	-14.5	-103.8
UNA-18-14	10/6/20	-14.5	-103.4
UNA-18-2	6/6/20	-12.9	-99.3
UNA-18-2	8/17/20	-14.1	-103.2
UNA-18-2	10/6/20	-14.4	-105.0
UNA-18-7	6/6/20	-13.5	-101.4
UNA-18-7	8/17/20	-14.4	-105.0
UNA-18-7	10/6/20	-14.6	-106.1
UNA-18-10	6/6/20	-13.6	-100.5
UNA-18-10	8/17/20	-14.4	-105.1
UNA-18-10	10/6/20	-14.7	-106.7
UNA-18-11	6/7/20	-14.6	-111.3
UNA-18-11	8/17/20	-15.4	-112.6
UNA-18-11	10/6/20	-15.4	-112.8
UNA-18-12-1	6/7/20	-14.3	-108.7

UNA-18-12-1	8/17/20	-14.6	-108.9
UNA-18-12-1	10/6/20	-14.8	-109.8
UNA 19	6/6/20	-14.4	-104.9
UNA 19	8/17/20	-14.7	-105.5
UNA 19	10/6/20	-14.8	-105.9
UNA 20	6/6/20	-13.6	-102.4
UNA 20	8/17/20	-14.0	-102.8
UNA 20	10/6/20	-14.0	-102.9

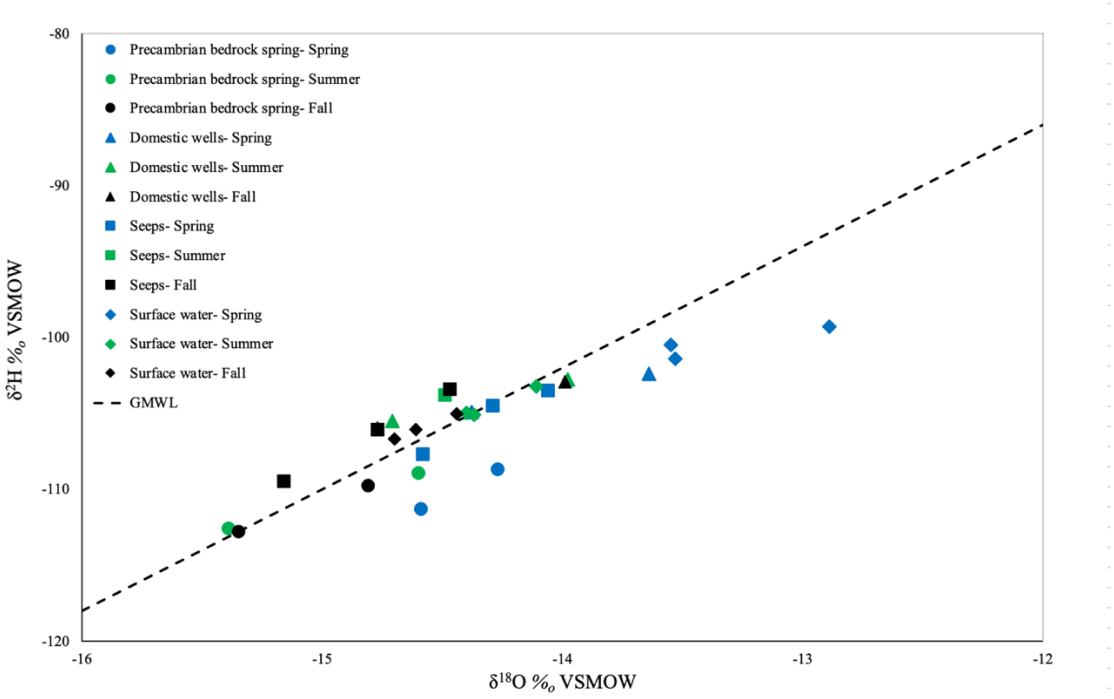

Figure 15. Relationship between $\delta^{18}O$ and $\delta^{2}H$ against the GMWL for samples collected in 2020. Results shown are grouped by site type and season to show seasonality effects on the isotopic composition of groundwater and surface water.

In general, the Precambrian bedrock spring samples, seeps and domestic well were observed to be generally more depleted with respect to $\delta^{18}O$ and $\delta^{2}H$ whereas West Creek samples

were more enriched in the heavier isotopes during the spring, summer, and fall. This fractionation effect is most likely as a result of snowmelt and/or evaporation in the spring. However, the expected snowmelt isotopic signature was likely attenuated due to drought conditions.

4.3. Statistical Analysis

PCA plots were created using $\delta^{18}O$, $\delta^{2}H$, the sum of major cations (ΣCa, Mg, K, Na), DOC, alkalinity and uranium for all the sites (Appendix 9) which were chosen because they best represent variability attributable to seasonality and groundwater source as noted previously. From Figure 11, U and the major cations are observed to vary between groundwater and West Creek whereas isotopes will show variability due to seasonality. Alkalinity (Fig. 10c) and DOC (Appendix A) is significantly different in the West Creek samples, seeps, domestic wells and Precambrian bedrock samples. PCA is a widely applied multivariate data analysis method that provides insight into the structure and relationships between the variables of a set of data (Jolliffe, 1986). The two principal components accounted for 81.52% of the total variance in the hydrochemical data (Fig. 16).

The first component (PC1) explains 58.51% of the total variance while PC2 explains 23.11% of the total variance. Primarily, the Precambrian bedrock spring samples are influenced mostly by the water chemistry such as the sum of the major cations. Whereas seasonal differences represented by $\delta^{18}O$, $\delta^{2}H$, and DOC factor into the distribution of West Creek and shallow groundwater. For example, in the spring, the isotopic composition and DOC concentration caused a shift of the surface water spring samples to the right side of the plot, related to snowmelt. The fall and summer stream samples cluster with the domestic well and seeps that is a result of baseflow condition.

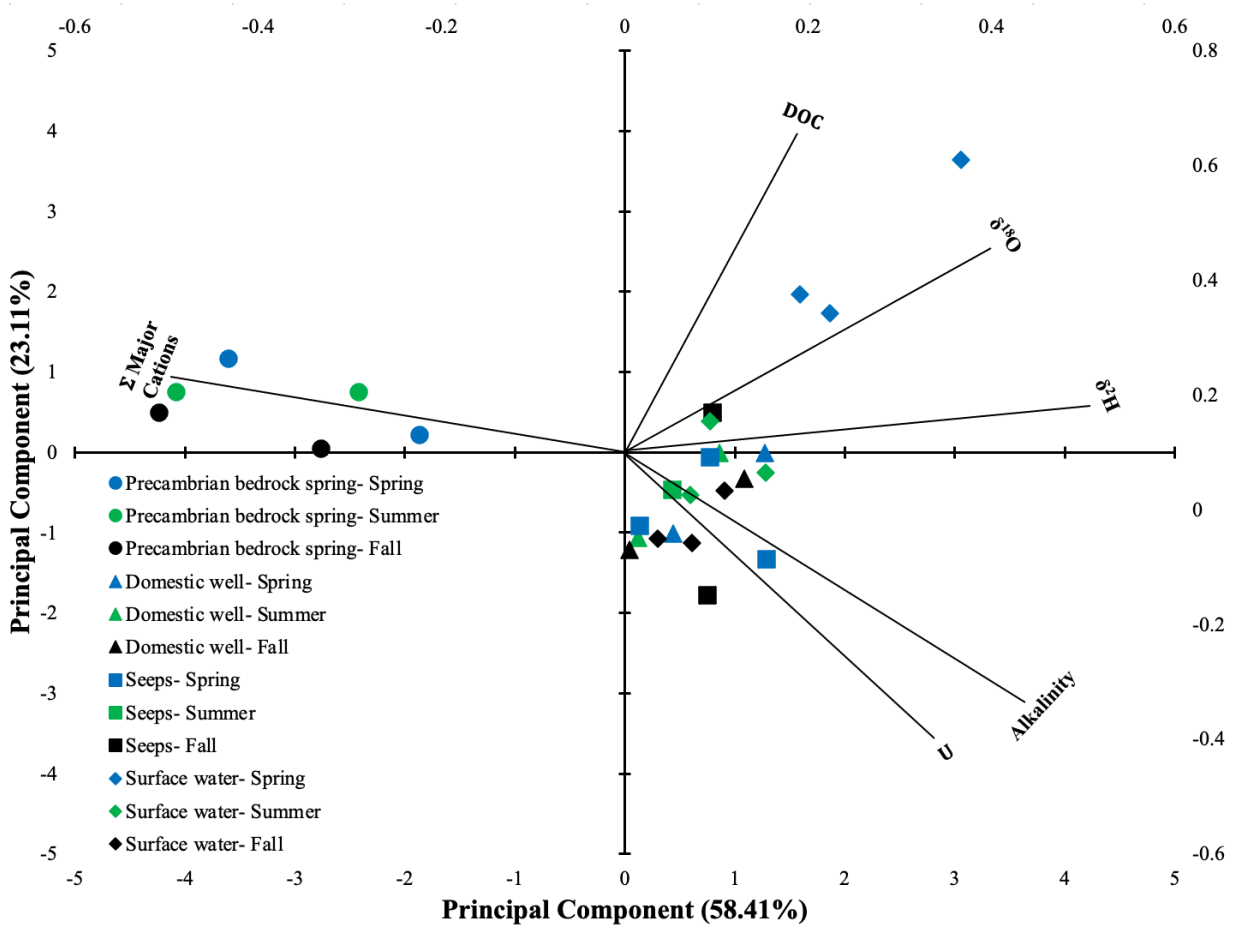

Figure 16. Principle Component Analysis plot showing select loading compoenents of DOC, alkalinity, uranium, stable istopes (δ18O and δ2H), and the sum of major cation (ΣMajor Cations) and PCA results for sites sampled in this study.

Spearman's correlations were calculated using the same data set for PCA (Appendix B). The Spearman's rank correlation (r) provides insight into the interrelationship distribution between two distinct variables. For this study, an r value greater than 0.5 indicates a strong correlation, r value between ± 0.30 and ± 0.49 indicates a moderate correlation and <0.29 indicates a weak correlation. Spearman's correlation results are shown in Table 4 as a matrix relating paired parameters to season and sample type. Strong correlations that include stable isotopes and DOC is likely related to seasonality whereas groundwater source is defined by correlations that include

cations and to a certain degree stable isotope, DOC and U. For example, the correlation between $\delta^{18}O$ – DOC is high in the spring (0.80) but decreases in the summer (-0.23) and fall (0.04), most likely due to snowmelt in the spring and baseflow conditions in the summer and fall. Whereas $\delta^{18}O$ - Sum of Major Cations, DOC - Sum of Major Cations and $\delta^{2}H$ – Alkalinity have much r values in the Precambrian bedrock spring samples when compared to the r values of the other sites combined together.

Table 4. Spearman´s rank correlation matrix, illustrating the relationship between the 6 variables used to create the PCA plot. Blue signifies strongcorrelation (r value greater than 0.5), green signifies a moderate correlation (r value between ± 0.30 and ± 0.49) and grey signifies weak correlation (r value <0.29).

	Spearman's Correlation				
	Spring	**Summer**	**Fall**	**Precambrian bedrock**	**Surface water+ Domestic well+ Seeps**
$\delta^{18}O$ - $\delta^{2}H$	0.88	0.91	0.90	0.88	0.92
$\delta^{18}O$ - Alkalinity	0.24	0.60	0.72	0.39	-0.29
$\delta^{18}O$ - DOC	0.80	-0.23	0.04	-0.77	0.65
$\delta^{18}O$ - Uranium	0.01	0.65	0.24	0.84	-0.33
$\delta^{18}O$ - Sum of Major Cations	-0.45	-0.82	-0.74	-0.67	-0.12
$\delta^{2}H$ - Alkalinity	0.55	0.87	0.93	0.48	-0.16
$\delta^{2}H$ - DOC	0.64	-0.33	0.24	-0.81	0.60
$\delta^{2}H$ - Uranium	0.28	0.72	0.41	0.97	-0.50

δ^2H - Sum of Major Cations	-0.77	-0.95	-0.89	-0.93	0.02
Alkalinity - Sum of Major Cations	-0.79	-0.84	-0.92	-0.48	0.72
Alkalinity - Uranium	0.38	0.68	0.60	0.29	-0.25
Alkalinity - DOC	-0.04	-0.29	0.39	-0.46	-0.33
DOC - Sum of Major Cations	-0.24	0.27	-0.08	-0.92	-0.13
DOC - Uranium	0.12	0.18	-0.07	0.84	-0.09
Uranium - Sum of Major Cations	-0.60	-0.80	-0.68	-0.83	-0.09

5. DISCUSSION

5.1 Water Chemistry of Streams and Groundwater in Unaweep Canyon

In-situ water chemistry (pH, temperature, conductivity, ORP, and alkalinity) in Unaweep Canyon generally does not show (Figure 10) any distinct water chemistry differences among the water samples. However, conductivity values do vary as the Precambrian bedrock spring samples exhibit nearly order-of-magnitude larger values (mean = 2037 µS/cm) than the West Creek and shallow groundwater readings (West Creek mean = 416 µS/cm; Well mean = 425 µS/cm; and seep mean = 433 µS/cm). The high conductivity values as well as cation concentrations are related to water-rock interaction processes, such as mineral weathering and cation exchange (Valett et al., 1996, Soulsby et al., 1999, Chapman et al., 2003, Modibo et al., 2019, Zhang et al., 2020). These cation concentrations are typically reflections of the water's residence time as it flows through the

aquifer medium (Wen et al., 2007). The Precambrian bedrock spring samples generally have higher ionic concentration related to the dissolution of minerals owing to prolonged water-rock reactions along the groundwater flow path. The higher conductivity (Fig. 10) in the Precambrian bedrock spring sites signifies a higher concentration of ions when compared to West Creek (mean = 354 µS/cm) and the shallow groundwater (mean = 376 µS/cm) sites. The ion-rich Precambrian bedrock spring samples also have a greater mean temperature (16.6ºC) when compared to West Creek (15.4 ºC) and the shallow groundwater (a median value of 13.05 ºC) sites. The reason for the high temperatures of the Precambrian bedrock spring samples may be due to the groundwater originating from a greater depth that in effect, increases the dissolution rate of minerals releasing more ions into groundwater and increasing conductivity (USGS, 2021). The relationship between water chemistry and groundwater-mineral interactions are further supported by PCA plots (Fig. 16). It appears that the Precambrian bedrock spring results group towards the major cations whereas the isotopes and DOC do not factor in the variability of the Precambrian samples since there is not much change in its isotopic compositions and DOC concentrations in the different seasons. The strong influence of major cations is also supported by Spearman correlation where the sum of major cations when paired with any other parameter exhibits very strong correlation and is significant (p-values < 0.005) when compared to the combination of all the other sites (Table 3; Appendix B). For example, δ^2H - Sum of Major Cations had an r value of -0.93 and p value of 0.00747 for the Precambrian bedrock spring samples, while the combination of all the other sites has an r value of 0.02 and p value of 0.9376.

Similar water chemistry between the seeps and domestic wells suggest that shallow groundwater is likely discharging at the seep sites. Seeps are generally groundwater that makes its way to the earth's surface (O'Driscoll et al., 2019); therefore, the seeps and domestic wells likely

originate from the same water source (Fig. 10), ion chemistry (Fig. 11&12) and similarity in water type based on the Piper plot (Fig. 13). For example, the seeps have a mean temperature of 16.7 ^{o}C while the domestic wells have a mean temperature of 17.1 ^{o}C, the seeps have a mean K^{+} concentration of 2.3 mg/L while the domestic well have a mean concentration of 1.9 mg/L Although the water table in Unaweep Canyon has not been fully investigated, personal communications with local residents suggest that the groundwater table is likely shallow at a depth of a couple of feet especially near the seeps and western West Creek. The water table depth was obtained via correspondence with Fred Bolton, a local in the area from whose well we sampled (UNA 20).

West Creek (surface water), domestic wells and seeps generally have lower ion concentrations compared to Precambrian bedrock spring samples as shown by the piper plot, and conductivity values (Figure10, 13; Table 2). This signifies a shorter residence time and potentially less mineral dissolution (Winnick et al., 2017, Carroll et al., 2018), as shown by the Piper plot, and conductivity values (Figure10, 13; Table 2). Therefore, the likely source of major ions may be from the dissolution of the mass wasting deposits in the canyon and streams. Other possible sources of major ions include anthropogenic activities, mainly from agricultural activities such as the use of manure and fertilizers for crop production (Ogrinc et al., 2019, Torres-Martínez et al., 2021), but there were no considerable concentrations of phosphate (PO_4^{3-}) and nitrate (NO_3^{-}) concentration in West Creek, seeps and domestic wells to support this suggestion. Nonetheless, the similarity in ion concentrations as evidenced in the piper plots between the domestic wells and West Creek demonstrates possible surface water- groundwater interaction as seen in the box plots in Figure 13. Dano (2010), in a study within a similar watershed in Nevada, also showed a link between surface water and groundwater due to the similarities in their ionic concentrations as

evidenced by piper plots (Fig. 13) and a surface water-groundwater interaction was suggested, which is similar to this study area.

The Piper plots (Fig. 13) also indicate that the Precambrian bedrock spring sample with a mixed water type reflects multiple processes in its evolution (Vasu et al., 2017), while the other Ca-Cl water type for the Precambrian is most likely due to the alteration of calcium-containing minerals such as aluminosilicates (Modibo et al., 2019). In contrast, West Creek, seeps and domestic well samples have Mg-HCO_3 water type with their neutral pH (Table 2) confirming that these waters are bicarbonate-dominated water sources. The Mg^{2+} likely reflects hydrolysis of ferromagnesian minerals (Modibo et al., 2019), and is confirmed from the presence of ferromagnesian minerals such as olivines, biotite and pyroxenes in the Precambrian rock samples from Unaweep Canyon (Case, 1991). Unpublished works have suggested the presence of a ton of biotite in the sediments found at the canyon. There are calcisols in the watershed (Marra, 2008); however more investigation would need to be done to confirm if they are a significant source of carbonate. Rather, bicarbonate in water likely relates to the weathering of plagioclase feldspar (Modibo et al., 2019) which occurs in the Precambrian bedrock which should produce a higher bicarbonate concentration, but the Precambrian bedrock spring's low alkalinity means that it may be forming complexes with other ions such as oxides (Liu et al., 2019). The presence of oxides in an unpublished whole-rock analysis of the Precambrian rocks in the canyon does support the possibility of bicarbonate ions forming complexes with these oxide ions.

Precambrian bedrock spring samples are isotopically lighter than the other samples, and groundwater originating from a deep source has been found by other studies to have more negative values of $\delta^{2}H$ and $\delta^{18}O$, indicating a colder climatic signal during recharge (Chen, 2001, Han et al., 2009). It is also possible that the Precambrian spring samples may have been recharged from

another source outside of the study area (Abd El-Samei, 1995, Abd El Samei and Sadek, 2001). Meanwhile, to confirm the former, more research would be needed as other processes that affect isotopes in rainfall, such as the altitude effect, would have to be considered, and a local meteoric water line would have to be generated for the canyon and surrounding areas. Although, based on results reported in other studies (Han et al., 2009, Yin et al., 2011), the suggestion that the Precambrian bedrock spring samples are originating from a deeper aquifer is more realistic owing to its much lighter isotopic signature (Sippel et al., 2020). However, to confirm this relationship, age dating of the water would be required. The seeps, West Creek and domestic wells are similar in isotopic compositions (Appendix A), indicating that they are recharged from the same source, and that source may be snowmelt, but the lack of the isotopic composition of snowpack and snowmelt data precludes a definite conclusion. The similarity in isotopic composition (West Creek and the domestic wells having mean $\delta^{18}O$ and $\delta^{2}H$ values of -14.7‰ and -106.68‰, -14.77‰ and 105.94‰ respectively) also suggests groundwater discharge is evident in baseflow.

Enrichment of both LREEs and MREEs in the surface water samples is typical among most streams (Dia et al., 2000, Hagedorn et al., 2011, Duvert et al., 2015). Lawrence et al. (2006), in their study on the REE variability in Southeast Queensland rivers, noticed an enrichment in MREEs and suggested that it was due to preferential weathering of phosphatic minerals from a source of phosphate which corresponded with the results of another study by Hannigan and Sholkovitz (2001). However, since there is no confirmed presence of a substantial phosphate source (Case, 1991) in the mass wasted deposits in and around West Creek, this is unlikely. Positive Ce anomaly and preferential removal of MREE from solution by co-precipitation on Fe-Mn oxides resulting in the LREE enrichment has also been noticed in surface waters (Pokrovsky and Schott, 2002, Leybourne and Johannesson, 2008, Mimba et al., 2020). But this is typical of

waters in reducing environments which is not the case for West Creek. Davranche et al. (2004), (2011) also highlighted that MREE enrichment could be due to complexation reactions with humic substances in organic-rich waters. Since electronegativity of ligands decreases as pH increases, fixed REEs bonded to organic matter release into solution as dissolved REEs (Pourret et al., 2007, Tang and Johannesson, 2010, Chen et al., 2017). This could be responsible for the spike in LREE concentrations in that one West Creek spring site (UNA-18-10) because of its substantial (4.2mg/L) spring DOC concentration. However, more studies investigating LREE behavior at DOC concentrations between 1-10mg/L; most studies have used much higher DOC concentrations. Another explanation could be the preferential fractionation of LREE to colloids as compared with HREEs (Sholkovitz et al., 1992, Lawrence et al., 2006). However, colloidal organic carbon was not collected at West Creek and no data are available. Nonetheless, Yan et al. (2018) demonstrated that colloidal organic carbon is ubiquitously present in surface waters at concentrations (13.6 TgC $year^{-1}$). Furthermore, snowmelt typically introduces a lot of organic matter into streams as evidenced by the strong correlation of $\delta^{18}O$ and DOC in the spring season (Table 6), suggesting DOC causes the spring spike in LREEs. Lawrence et al. (2006) has observed that in circumneutral river waters, LREE and HREE form stable complexes with bicarbonate ions, resulting in a relatively conservative REE behavior. This is noticed in every other West Creek samples except from UNA-18-10 in the spring.

The domestic wells and seeps have a slight increase in MREEs compared to LREEs (Fig. 14). Studies have suggested this behavior resultants from effect of string complexation of REE with carbonate, especially as a dicarbonato complex ($REE(CO_3)_2^-$) which occurs as pH becomes more basic (Wood, 1990, Millero, 1992, Johannesson et al., 1995). This is due to REE forming a progressively stronger bond as the atomic number increases (Choi et al., 2009) and thus greater

complexation/solubility of the MREEs. Although a relationship between West Creek and groundwater has been established earlier on, the interaction might have been masked by the much higher DOC and pH content of surface water which then causes more pronounced fractionation between the REEs.

Furthermore, the Precambrian bedrock spring samples exhibit little to no fractionation, and their REE concentrations and ratios are much lower than that of the West Creek samples (Fig. 14). The absence of Ce anomalies in the Precambrian bedrock spring samples supports the findings of other authors who also reported the same for groundwater originating from bedrock aquifers (Göb et al., 2013, Yan et al., 2013) Unpublished whole-rock analysis however does not support the REE pattern observed as there appears to be higher concentrations of whole rock LREE when compared to HREE which should lead to more dissolved LREEs than HREEs. The fractionation in the whole-rock analysis has been identified to be as a result of the presence of zircon or garnet in igneous rocks which tends to incorporate HREE into its crystal structure (Rollison, 1994), and the whole-rock analysis does show a considerable amount of zircon present in the Precambrian bedrock rock samples. Additionally, preferential dissolution of LREE containing minerals over HREE containing minerals has been shown to influence their groundwater abundances (Harlavan and Erel, 2002). And although this means that the Precambrian bedrock spring samples should have much higher LREE concentrations, studies have shown that with increasing pH, LREE depletion occurs due to adsorption of LREE onto oxide surfaces, which could explain why the concentration of LREE is much lower and similar to that of the HREE (Elderfield et al., 1990, Smedley, 1991, Dupré et al., 1996, Leybourne et al., 2000). And the unpublished whole-rock analyses mentioned above does show the presence of substantial oxide minerals to support this suggestion.

5.2 Seasonality

Changes in pH may also be a result of seasonal variations particularly in watersheds with acute sources including seasonal snowmelt. Seasonal variation in pH often factors into the weathering pattern and concentration of dissolved solutes in surface water (Anshumali and Ramanathan, 2007). During snowmelt or when water is moving through a watershed, solute concentration tends to become more dilute when compared to solute concentrations during baseflow conditions, which mainly related to the large volume of meltwater moving through the streams and groundwater and including longer residence times. Deka et al. (2015) reported very little to no seasonal variation in surface water ion chemistry for pre-monsoon and post-monsoon seasons, due to surface water chemistry in high altitude regions largely depending on snowmelt quality and the terrain in which the meltwater traveled. However, ion chemistry in Unaweep canyon did show seasonal variation where the spring samples were lower in concentration (~ 10-20% difference) than the summer and fall samples which is most likely due to the influence of snowmelt in the spring and baseflow conditions in the summer and fall (Appendix A). Spearman's correlation results support this observation where in the spring, the sum of major cations when paired with any other parameter had a much lower correlation when compared with the correlation values in the summer and fall (Table 3). For example, $\delta^{18}O$ - Sum of Major Cations had an r value of -0.45 in the spring, -0.82 in the summer and -0.74 in the fall. Studies in snow-dominated watersheds have also reported such variation in the ion concentration of streams to be significantly lower during snowmelt conditions and higher during baseflow (Winnick et al., 2017, Carroll et al., 2018). Thomas et al. (2014) also observed a depletion in ion concentration during monsoons due to enhanced dilution with much higher concentrations post and pre-monsoon in India's Muthirapuzha River Basin. For example, in Thomas et al. (2014), the $H_4SiO_{4/}(Na^+ + K^+)$ ratio that

was suggested by the study to signify silicate weathering had a 23% and 92% difference between the monsoon and pre-monsoon season respectively. Although this study showed a higher percent differences in the ion chemistry concentration between spring and baseflow conditions when compared to this study, precipitation (as snow) was significantly higher (an order of 1 magnitude) in the Muthirapuzha River basin than in Unaweep Canyon. Therefore, sampling would need to be carried out in an average precipitation year to get a better grasp of the relationship between snowmelt and solute concentration in the canyon.

In terms of seasonality, the isotopic composition due to fractionation seemed to affect all the water samples collected at the study site; however, a shift was only pronounced in the springtime (Fig. 15). All the samples collected in the spring are seen to deviate from the GMWL, and this may be due to the melt-out effect or sublimation of snow (Ala-Aho et al., 2017); the latter is unlikely as snowpack was much lower in 2020 which caused snowmelt to occur much earlier in the year as seen in the hydrograph (Fig. 5). Early meltwater is generally isotopically lighter but as the melt progresses, both the residual snowpack and generated meltwater become isotopically heavier (Taylor et al., 2001, Dietermann and Weiler, 2013). This phenomenon is most likely true as the spring samples were sampled not long after snowmelt (Fig. 5) and the strong Spearman's correlation ($r = 0.80$) between $\delta^{18}O$ and DOC in the Spring suggests that snowmelt is mobilizing DOC along the pathway from soils to surface water. Such a relationship between the two parameters is also observed in the PCA plots where the spring surface water samples shift and cluster towards the $\delta^{18}O$ and DOC components (Fig 16).

Typically, stream samples representing the summer season are usually enriched with respect to the heavier isotopes, but this was not the case for the summer samples in this study as they plotted close to the GMWL (Fig. 15). Studies have shown that evaporation of surface water

in arid climates would cause shift of water samples from the GMWL (Dansgaard, 1964, Clark, 1987), which was not the case in summer samples in the study site, as their isotopic signatures were very similar (~ a 2% difference) to that of the fall samples (Fig. 15). The general similarity in the isotopic composition of the seeps, domestic wells and surface water in summer and fall samples suggest the recharging of surface water by groundwater which further supports the surface water-groundwater mixing mentioned in the section above. West Creek, the seeps and the domestic wells having average isotopic values of -14.07‰ $\delta^{18}O$ and -103.59‰ $\delta^{2}H$, 14.45‰ $\delta^{18}O$ and -105.42‰ $\delta^{2}H$, -14.25‰ $\delta^{18}O$ and 104.01‰ $\delta^{2}H$ respectively. From the hydrograph in figure 5, baseflow conditions began around July 2020 and the summer sampling did not take place until August, as well as the drought conditions of 2020 could be the reason for the similarity in the isotopic signatures. Liu et al. (2005) also noticed a mixing between surface water and groundwater due to similar isotopic signatures and ion chemistry following prolong dry seasons in the Huaishahe basin in Beijing, China.

5.3 Sources of Groundwater in Unaweep Canyon

The similarity in the chemistry and isotopic signatures of the seeps, and domestic well samples suggest the same water source, with groundwater discharge the likely source of water in West Creek during baseflow. The piper plot, isotope plot, ion chemistry and REE plots (Figures 10-15) also generally show mixing between these three water types with similar solute concentration and isotope values. The largest difference is fractionation of isotopes and REE that occurs in the surface water sites possibly due to its much lower alkalinity and greater DOC concentrations (Table 2) when compared to the seeps and domestic wells. In contrast, samples from the Precambrian bedrock springs may represent more than one source of deeper groundwater. The possibility of multiple groundwater sources flowing through the Precambrian basement is

evinced by variations in the piper plot, ion chemistry, isotope data and PCA plot of the different Precambrian bedrock samples (UNA-18-11 and UNA-18-12-1). Behm et al. (2019) through a P-wave velocity model for Unaweep Canyon the presence of water-saturated sediments in the overdeepened section of the valley floor. However, the slopes of the topography (NW-SE) of the canyon and the dip (East) of this interpreted saturated zone oppose each other, so the possible aquifer would have to either be confined or leaking through the fractured basement. The former was later confirmed when V_p/V_s ratios that were significantly higher where the lithology changes from the fanglomerate to the lacustrine sand. The indicated saturation in the lacustrine sand, confined by fine clayey sand has been confirmed by the generalized lithology of Massey core in the canyon (Fig. 3).

One possible explanation for the source of water originating from the Precambrian bedrock springs is that the springs are being fed by water from the lacustrine sand making its way through fractured Precambrian bedrock and reaching the surface as springs. However, the extent of the fractures and the groundwater flow directions are unknown. Alternatively, the Precambrian bedrock spring samples are being fed from a regional bedrock aquifer system related to groundwater fracture flow through the Precambrian basement rock (Colorado Geological Survey, 2017).

6. CONCLUSION

Water chemistry, REE and isotopic results indicate that Unaweep Canyon hosts multiple sources of groundwater that are not hydro-geochemically linked. The seeps in the Unaweep Canyon colluvium fill are connected to the shallow aquifer based on its similar chemistry to the domestic wells. The Precambrian bedrock spring sites have geochemical attributes of high ionic composition, flat REE patterns and generally much lighter isotopic signatures that hint at the

existence of groundwater from a deeper, bedrock aquifer. Based on a combination of core lithology from the Massey Core and recent shallow geophysical findings, a deeper, confined aquifer in Unaweep Canyon is hypothesized to exist below the colluvium deposits. However, testing whether this sand layer is the source of the water from the Precambrian bedrock springs and the mechanism behind its flow path requires more samples collected in an average precipitation year. This study uses non-invasive techniques to establish baseline data on aquifer systems that enables identification of multiple groundwater sources in Unaweep Canyon, although the component of seasonality in water chemistry and isotope data requires further work. This study demonstrated that this hydrogeochemical approach not only delineated multiple sources of groundwater but also provides insight into potential biogeochemical process that also influence water chemistry.

6.1 Recommendations for Future Research

Although this study successfully identified the existence of multiple sources of groundwater, the following recommendations should result in more effective data to resolve a lack of clear seasonal variations and provide more insight into the possible groundwater discharge from the confined aquifer.

- 2020 was a drought year, so seasonal effects on water chemistry and isotopes were attenuated and therefore, future studies should obtain data in an average precipitation year and for multiple years.
- Dating the water samples from the Precambrian bedrock spring samples and the lacustrine sand would confirm the presence of multiple sources of aquifers. Pore water directly from the lacustrine sand can be obtained if Unaweep canyon valley floor is being drilled and then dated.

- Additional sampling sites such as wells, seeps, springs and surface water sites would provide a more holistic representation.
- Sampling at snowmelt and baseflow conditions would better represent these conditions that greatly influence water chemistry and isotopes.
- Collecting water samples directly from the identified saturated lacustrine sand aquifer and comparing hydrogeochemical data with Precambrian bedrock spring samples to confirm if they are of the same source. This would involve drilling wells into the lacustrine sand and obtaining water samples directly from it.

References

ABD EL SAMEI, S. G. & SADEK, M. A. 2001. Groundwater recharge and flow in the lower Cretaceous Nubian sandstone aquifer in the Sinai Peninsula, using isotopic techniques and hydrochemistry. *Hydrogeol* 9**,** 378–389.

ABD EL-SAMEI, S. G. 1995. *Isotopic and hydrochemical studies on the groundwater of Sinai Peninsula (Dissertation). .* Ain Shams University,.

ABDELSHAFY, M., SABER, M., ABDELHALEEM, A., ABDELRAZEK, S. M. & SELEEM, E. M. 2019. Hydrogeochemical processes and evaluation of groundwater aquifer at Sohag city, Egypt. *Scientific African,* 6**,** e00196.

ALA-AHO, P., TETZLAFF, D., MCNAMARA, J. P., LAUDON, H., KORMOS, P. & SOULSBY, C. 2017. Modeling the isotopic evolution of snowpack and snowmelt: Testing a spatially distributed parsimonious approach. *Water resources research,* 53**,** 5813-5830.

ALY, A., ALOMRAN, A., ALWABEL. M, ALMAHAINI, A. & M, A. 2013. Hydrochemical and quality of water resources in Saudi Arabia groundwater: A comparative study of Riyadh and Al-Ahsa regions. *International Academy of Ecology and Environmental Sciences,* 3**,** 42-51.

AMELI, A. A., CRAIG, J. R. & MCDONNELL, J. J. 2015. Are all runoff processes the same? Numerical experiments comparing a Darcy-Richards solver to an overland flow-based approach for subsurface storm runoff simulation. *Water Resources Research,* 51**,** 10008-10028.

ANDERSON, S. P., DIETRICH, W. E., TORRES, R., MONTGOMERY, D. R. & LOAGUE, K. 1997. Concentration-discharge relationships in runoff from a steep, unchanneled catchment. *Water Resources Research,* 33**,** 211-225.

ANSHUMALI & RAMANATHAN, A. L. 2007. Seasonal variation in the major ion chemistry of Pandoh Lake, Mandi District, Himachal Pradesh, India. *Applied Geochemistry,* 22**,** 1736-1747.

BAGARD, M.-L., CHABAUX, F., POKROVSKY, O. S., VIERS, J., PROKUSHKIN, A. S., STILLE, P., RIHS, S., SCHMITT, A.-D. & DUPRÉ, B. 2011. Seasonal variability of element fluxes in two Central Siberian rivers draining high latitude permafrost dominated areas. *Geochimica et Cosmochimica Acta,* 75**,** 3335-3357.

BALCO, G., SOREGHAN, G. S., SWEET, D. E., MARRA, K. R. & BIERMAN, P. R. 2013. Cosmogenic-nuclide burial ages for Pleistocene sedimentary fill in Unaweep Canyon, Colorado, USA. *Quaternary Geochronology,* 18**,** 149-157.

BANNER, J. L., WASSERBURG, G. J., DOBSON, P. F., CARPENTER, A. B. & MOORE, C. H. 1989. Isotopic and trace element constraints on the origin and evolution of saline groundwaters from central Missouri. *Geochimica et Cosmochimica Acta,* 53**,** 383-398.

BARBIERI, M., BOSCHETTI, T., PETITTA, M. & TALLINI, M. 2005. Stable isotope (2H, 18O and 87Sr/86Sr) and hydrochemistry monitoring for groundwater hydrodynamics analysis in a karst aquifer (Gran Sasso, Central Italy). *Applied Geochemistry,* 20**,** 2063-2081.

BAU, M. & DULSKI, P. 1996. Anthropogenic origin of positive gadolinium anomalies in river waters. *Earth and Planetary Science Letters,* 143**,** 245-255.

BEHM, M., CHENG, F., PATTERSON, A. & SOREGHAN, G. S. 2019. Passive processing of active nodal seismic data: estimation of V _P/ V _S ratios to characterize structure and hydrology of an alpine valley infill. *Solid Earth,* 10**,** 1337-1354.

BJERG, P. L., HINSBY, K., CHRISTENSEN, T. H. & GRAVESEN, P. 1992. Spatial variability of hydraulic conductivity of an unconfined sandy aquifer determined by a mini slug test. *Journal of Hydrology,* 136**,** 107-122.

BROOKINS, D. G. 1989. Chapter 8. AQUEOUS GEOCHEMISTRY OF RARE EARTH ELEMENTS. *Geochemistry and Mineralogy of Rare Earth Elements.* De Gruyter.

CARRILLO-RIVERA, J. J., VARSÁNYI, I., KOVÁCS, L. Ó. & CARDONA, A. 2007. Tracing Groundwater Flow Systems with Hydrogeochemistry in Contrasting Geological Environments. *Water, Air, and Soil Pollution,* 184**,** 77-103.

CARROLL, R. W. H., BEARUP, L. A., BROWN, W., DONG, W., BILL, M. & WILLLAMS, K. H. 2018. Factors controlling seasonal groundwater and solute flux from snow-dominated basins. *Hydrological Processes,* 32**,** 2187-2202.

CASE, J. E. 1991. Geologic map of the northwestern part of the Uncompahgre Uplift, Grand County, Utah, and Mesa County, Colorado, with emphasis on Proterozoic rocks. US Geological Survey.

CASTOR, S. B. & HENDRICK, J. B. 2006. *Rare Earth Elements. ,* Littleton, Colorado, Society for Mining, Metallurgy, and Exploration.

CDSS. 2017. *HydroBase Point Data Well Applications* [Online]. Available: http://cdss.state.co.us/GIS/Pages/AllGISData.aspx. [Accessed].

CHACKO, T., COLE, D. R. & HORITA, J. 2001. Equilibrium Oxygen, Hydrogen and Carbon Isotope Fractionation Factors Applicable to Geologic Systems. *Reviews in Mineralogy and Geochemistry,* 43**,** 1-81.

CHAPAGAIN, S. K., SHRESTHA, S., NAKAMURA, T., PANDEY, V. P. & KAZAMA, F. 2009. Arsenic occurrence in groundwater of Kathmandu Valley, Nepal. *Desalination and Water Treatment,* 4**,** 248-254.

CHAPMAN, J. B., LEWIS, B. & LITUS, G. 2003. Chemical and isotopic evaluation of water sources to the fens of South Park, Colorado. *Environmental Geology,* 43**,** 533-545.

CHEN, L., MA, T., DU, Y. & XIAO, C. 2017. Dissolved Rare Earth Elements of Different Waters in Qaidam Basin, Northwestern China. *Procedia Earth and Planetary Science,* 17**,** 61-64.

CHEN, Z. Y. 2001. *Groundwater resources evolution based on paleoenvironmental information from groundwater system in North China Plain.* Ph.D, Jilin University.

CHOI, H.-S., YUN, S.-T., KOH, Y.-K., MAYER, B., PARK, S.-S. & HUTCHEON, I. 2009. Geochemical behavior of rare earth elements during the evolution of CO2-rich groundwater: A study from the Kangwon district, South Korea. *Chemical Geology,* 262**,** 318-327.

CLARK, I. D. 1987. *Groundwater resources in the Sultanate of Oman: origin, circulation times, recharge processes and paleoclimatology.* Ph.D., University de Paris-Sud, France

CLARK, I. D. & FRITZ, P. 1997. *Environmental isotopes in hydrogeology,* Boca Raton, FL, CRC Press/Lewis Publishers.

COLORADO GEOLOGICAL SURVEY. 2017. *OF-17-01 Geology and Groundwater Resources of Mesa County, Colorado.* [Online]. Golden, CO: Colorado Geological Survey. Available: https://coloradogeologicalsurvey.org/publications/geology-groundwater-resources-mesa-colorado [Accessed].

COLORADO STATE UNIVERSITY. 2019. *Colorado Climate Center* [Online]. Available: https://climate.colostate.edu/data_access.html [Accessed August 14th 2020].

COPLEN, T. B. 1994. Reporting of stable hydrogen, carbon, and oxygen isotopic abundances (Technical Report). *Pure and Applied Chemistry,* 66**,** 273-276.

COPLEN, T. B., HERCZEG, A. L. & BARNES, C. 2000. Isotope Engineering—Using Stable Isotopes of the Water Molecule to Solve Practical Problems. *Environmental Tracers in Subsurface Hydrology.* Springer US.

COSTANZA, R., D'ARGE, R., DE GROOT, R., FARBER, S., GRASSO, M., HANNON, B., LIMBURG, K., NAEEM, S., O'NEILL, R. V., PARUELO, J., RASKIN, R. G., SUTTON, P. & VAN DEN BELT, M. 1998. The value of ecosystem services: putting the issues in perspective. *Ecological Economics,* 25**,** 67-72.

CRAIG, H. 1961. Isotopic Variations in Meteoric Waters. *Science,* 133**,** 1702-3.

DANO, E. 2010. *Identification of geochemical facies through major ion data and additional parameters from shallow groundwater utilizing a comparison of geomathematics and traditional methods in Las Vegas Valley, Nevada.* Dissertations, UNLV Theses, Dissertations, Professional Papers, and Capstones.

DANSGAARD, W. 1964. Stable isotopes in precipitation. *Tellus,* 16**,** 436-468.

DAVRANCHE, M., GRYBOS, M., GRUAU, G., PÉDROT, M., DIA, A. & MARSAC, R. 2011. Rare earth element patterns: A tool for identifying trace metal sources during wetland soil reduction. *Chemical Geology,* 284**,** 127-137.

DAVRANCHE, M., POURRET, O., GRUAU, G. & DIA, A. 2004. Impact of humate complexation on the adsorption of REE onto Fe oxyhydroxide. *Journal of Colloid and Interface Science,* 277**,** 271-279.

DEKA, J. P., TAYENG, G., SINGH, S., HOQUE, R. R., PRAKASH, A. & KUMAR, M. 2015. Source and seasonal variation in the major ion chemistry of two eastern Himalayan high altitude lakes, India. *Arabian Journal of Geosciences,* 8**,** 10597-10610.

DIA, A., GRUAU, G., OLIVIÉ-LAUQUET, G., RIOU, C., MOLÉNAT, J. & CURMI, P. 2000. The distribution of rare earth elements in groundwaters: assessing the role of source-rock composition, redox changes and colloidal particles. *Geochimica et Cosmochimica Acta,* 64**,** 4131-4151.

DIETERMANN, N. & WEILER, M. 2013. Spatial distribution of stable water isotopes in alpine snow cover. *Hydrol. Earth Syst. Sci.,* 17**,** 2657-2668.

DOMENICO, P. A. & SCHWARTZ, F. W. 1991. *Physical and Chemical Hydrogeology,* New York, John Wiley & Sons.

DOYLE, G., ROCCHIO, J. & CULVER, J. 2002. Survey of Seeps and Springs within the Bureau of Land Management's Grand Junction Field Office Management Area (Mesa County, CO) *In:* UNIVERSITY, C. S. (ed.) *Colorado Natural Heritage Program.*

DUPRÉ, B., GAILLARDET, J., ROUSSEAU, D. & ALLÈGRE, C. J. 1996. Major and trace elements of river-borne material: The Congo Basin. *Geochimica et Cosmochimica Acta,* 60**,** 1301-1321.

DUVERT, C., CENDÓN, D. I., RAIBER, M., SEIDEL, J.-L. & COX, M. E. 2015. Seasonal and spatial variations in rare earth elements to identify inter-aquifer linkages and recharge processes in an Australian catchment. *Chemical Geology,* 396**,** 83-97.

DWIVEDI, D., STEEFEL, C. I., ARORA, B., NEWCOMER, M., MOULTON, J. D., DAFFLON, B., FAYBISHENKO, B., FOX, P., NICO, P., SPYCHER, N., CARROLL, R. & WILLIAMS, K. H. 2018. Geochemical Exports to River From the Intrameander Hyporheic

Zone Under Transient Hydrologic Conditions: East River Mountainous Watershed, Colorado. *Water Resources Research,* 54**,** 8456-8477.

ELDERFIELD, H., UPSTILL-GODDARD, R. & SHOLKOVITZ, E. R. 1990. The rare earth elements in rivers, estuaries, and coastal seas and their significance to the composition of ocean waters. *Geochimica et Cosmochimica Acta,* 54**,** 971-991.

EXNER-KITTRIDGE, M., STRAUSS, P., BLÖSCHL, G., EDER, A., SARACEVIC, E. & ZESSNER, M. 2016. The seasonal dynamics of the stream sources and input flow paths of water and nitrogen of an Austrian headwater agricultural catchment. *Science of The Total Environment,* 542**,** 935-945.

FARID, I., ZOUARI, K., RIGANE, A. & BEJI, R. 2015. Origin of the groundwater salinity and geochemical processes in detrital and carbonate aquifers: Case of Chougafiya basin (Central Tunisia). *Journal of Hydrology,* 530**,** 508-532.

FONTES, J. C. 1980. *Environmental isotopes in groundwater hydrology,* Netherlands, Elsevier.

GAT, J. R. 1996. OXYGEN AND HYDROGEN ISOTOPES IN THE HYDROLOGIC CYCLE. *Annual Review of Earth and Planetary Sciences,* 24**,** 225-262.

GIBSON, H. D., BROWN, R. L. & CARR, S. D. 2005. U–Th–Pb geochronologic constraints on the structural evolution of the Selkirk fan, northern Selkirk Mountains, southern Canadian Cordillera. *Journal of Structural Geology,* 27**,** 1899-1924.

GÖB, S., LOGES, A., NOLDE, N., BAU, M., JACOB, D. E. & MARKL, G. 2013. Major and trace element compositions (including REE) of mineral, thermal, mine and surface waters in SW Germany and implications for water–rock interaction. *Applied Geochemistry,* 33**,** 127-152.

GODSEY, S. E., KIRCHNER, J. W. & CLOW, D. W. 2009. Concentration-discharge relationships reflect chemostatic characteristics of US catchments. *Hydrological Processes,* 23**,** 1844-1864.

GRUAU, G., DIA, A., OLIVIÉ-LAUQUET, G., DAVRANCHE, M. & PINAY, G. 2004. Controls on the distribution of rare earth elements in shallow groundwaters. *Water Research,* 38**,** 3576-3586.

GURRIERI, J. T. & FURNISS, G. 2004. Estimation of groundwater exchange in alpine lakes using non-steady mass-balance methods. *Journal of Hydrology,* 297**,** 187-208.

HAGEDORN, B., CARTWRIGHT, I., RAVEGGI, M. & MAAS, R. 2011. Rare earth element and strontium geochemistry of the Australian Victorian Alps drainage system: Evaluating the dominance of carbonate vs. aluminosilicate weathering under varying runoff. *Chemical Geology,* 284**,** 105-126.

HAN, D., LIANG X FAU - JIN, M., JIN M FAU - CURRELL, M. J., CURRELL MJ FAU - HAN, Y., HAN Y FAU - SONG, X. & SONG, X. 2009. Hydrogeochemical indicators of groundwater flow systems in the Yangwu River alluvial fan, Xinzhou Basin, Shanxi, China.

HANNIGAN, R. E. & SHOLKOVITZ, E. R. 2001. The development of middle rare earth element enrichments in freshwaters: weathering of phosphate minerals. *Chemical Geology,* 175**,** 495-508.

HARLAVAN, Y. & EREL, Y. 2002. The release of Pb and REE from granitoids by the dissolution of accessory phases. *Geochimica et Cosmochimica Acta,* 66**,** 837-848.

HAZEN, J. M., WILLIAMS, M. W., STOVER, B. & WIREMAN, M. 2002. Characterization of acid mine drainage using a combination of hydrometric, chemical and isotopic analyses, Mary Murphy Mine, Colorado. . *Environmental Geochemistry and Health,* 24**,** 1-22.

HOOD, U. C. 2011. Unaweep Canyon—Which river ran through it? *Mountain Geologist,* 48**,** 45-57.

HORNBERGER, G. M., SCANLON, T. M. & RAFFENSPERGER, J. P. 2001. Modelling transport of dissolved silica in a forested headwater catchment: the effect of hydrological and chemical time scales on hysteresis in the concentration-discharge relationship. *Hydrological Processes,* 15**,** 2029-2038.

IMES, J. L. & WOOD, W. W. 2007. Solute and isotope constraint of groundwater recharge simulation in an arid environment, Abu Dhabi Emirate, United Arab Emirates. *Hydrogeology Journal,* 15**,** 1307-1315.

INGRI, J., WIDERLUND, A., LAND, M., GUSTAFSSON, Ö., ANDERSSON, P. & ÖHLANDER, B. 2000. Temporal variations in the fractionation of the rare earth elements in a boreal river; the role of colloidal particles. *Chemical Geology,* 166**,** 23-45.

IPCC 2014. IPCC report calls for action to limit health impacts of climate change. *The Pharmaceutical Journal*.

JOHANNESSON, K. H., STETZENBACH, K. J. & HODGE, V. F. 1995. Speciation of the rare earth element neodymium in groundwaters of the Nevada Test Site and Yucca Mountain and implications for actinide solubility. *Applied Geochemistry,* 10**,** 565-572.

JOHANNESSON, K. H., STETZENBACH, K. J. & HODGE, V. F. 1997. Rare earth elements as geochemical tracers of regional groundwater mixing. *Geochimica et Cosmochimica Acta,* 61**,** 3605-3618.

JOLLIFFE, I. T. 1986. Principal Component Analysis and Factor Analysis. *Principal Component Analysis.* Springer New York.

KIM, H., DIETRICH, W. E., THURNHOFFER, B. M., BISHOP, J. K. B. & FUNG, I. Y. 2017. Controls on solute concentration-discharge relationships revealed by simultaneous hydrochemistry observations of hillslope runoff and stream flow: The importance of critical zone structure. *Water Resources Research,* 53**,** 1424-1443.

KUMAR, M., RAMANATHAN, A. L., RAO, M. S. & KUMAR, B. 2006. Identification and evaluation of hydrogeochemical processes in the groundwater environment of Delhi, India. *Environmental Geology,* 50**,** 1025-1039.

KUMAR, P. J. 2016. Influence of water level fluctuation on groundwater solute content in a tropical south Indian region: a geochemical modelling approach. *Modeling Earth Systems and Environment,* 2**,** 1-9.

LAWRENCE, M. G., GREIG, A., COLLERSON, K. D. & KAMBER, B. S. 2006. Rare Earth Element and Yttrium Variability in South East Queensland Waterways. *Aquatic Geochemistry,* 12**,** 39-72.

LEYBOURNE, M. I., GOODFELLOW, W. D., BOYLE, D. R. & HALL, G. M. 2000. Rapid development of negative Ce anomalies in surface waters and contrasting REE patterns in groundwaters associated with Zn–Pb massive sulphide deposits. *Applied Geochemistry,* 15**,** 695-723.

LEYBOURNE, M. I. & JOHANNESSON, K. H. 2008. Rare earth elements (REE) and yttrium in stream waters, stream sediments, and Fe–Mn oxyhydroxides: Fractionation, speciation, and controls over REE+Y patterns in the surface environment. *Geochimica et Cosmochimica Acta,* 72**,** 5962-5983.

LI, Z., GUI, J., WANG, X., FENG, Q., ZHAO, T., OUYANG, C., GUO, X., ZHANG, B. & SHI, Y. 2019. Water resources in inland regions of central Asia: Evidence from stable isotope tracing. *Journal of Hydrology,* 570**,** 1-16.

LIU, H., GUO, H., POURRET, O., CHEN, Y. & YUAN, R. 2019. Role of Manganese Oxyhydroxides in the Transport of Rare Earth Elements Along a Groundwater Flow Path. *International journal of environmental research and public health,* 16**,** 2263.

LIU, X. C., XIA, J., SONG, X. F., YU, J. J., TANG, C. Y. & ZHAN, C. S. 2005. Study of Surface Water and Groundwater Using Isotopes in Huaishahe Basin in Beijing, China.

. *Seventh IAHS Scientific Assembly.* Beijing.

MAINEULT, A., STROBACH, E. & RENNER, J. 2008. Self-potential signals induced by periodic pumping tests. *Journal of Geophysical Research,* 113.

MANKIN, J. S., VIVIROLI, D., SINGH, D., HOEKSTRA, A. Y. & DIFFENBAUGH, N. S. 2015. The potential for snow to supply human water demand in the present and future. *Environmental Research Letters,* 10**,** 114016.

MARÉCHAL, J. C. & ETCHEVERRY, D. 2003. The use of 3 H and 18 O tracers to characterize water inflows in Alpine tunnels. *Applied Geochemistry,* 18**,** 339-351.

MARKS, M. B., KIRK, A. R. & CORMIER, M. 2008. Assessment and Closure of the Glengarry Adit, New World Mining District, Cooke City, Montana. *Journal American Society of Mining and Reclamation,* 2008**,** 628-661.

MARRA, J. 2008. *Late Cenozoic geomorphic and climatic evolution of the northeastern Colorado Plateau as recorded by Plio-Pleistocene sediment fill in Unaweep Canyon, Colorado* Masters, University of Oklahoma.

MATTHESS, G. 1982. *The properties of ground water* New York, NY, John Wiley and Sons.

MAZOR, E. 1991. *Applied Chemical and Isotopic Groundwater Hydrology,* Suffolk, Va, Open University Press.

MCDONNELL, J. J. & BEVEN, K. 2014. Debates-The future of hydrological sciences: A (common) path forward? A call to action aimed at understanding velocities, celerities and residence time distributions of the headwater hydrograph. *Water Resources Research,* 50**,** 5342-5350.

MEKONNEN, M. M. & HOEKSTRA, A. Y. 2016. Four billion people facing severe water scarcity. *Sci Adv,* 2**,** e1500323.

MESA COUNTY 2019. Growth.

MILLERO, F. J. 1992. Stability constants for the formation of rare earth-inorganic complexes as a function of ionic strength. *Geochimica et Cosmochimica Acta,* 56**,** 3123-3132.

MIMBA, M. E., WIRMVEM, M. J., NGUEMHE FILS, S. C., NUMANAMI, N., NFORBA, M. T., OHBA, T., AKA, F. T. & SUH, C. E. 2020. Geochemical Behavior of REE in Stream Water and Sediments in the Gold-Bearing Lom Basin, Cameroon: Implications for Provenance and Depositional Environment. *Aquatic Geochemistry,* 26**,** 53-70.

MODIBO, S. A., LIN, X. & KONÉ, S. 2019. Assessing Groundwater Mineralization Process, Quality, and Isotopic Recharge Origin in the Sahel Region in Africa. *Water,* 11**,** 789.

MÖLLER, P., KNAPPE, A. & DULSKI, P. 2014. Seasonal variations of rare earths and yttrium distribution in the lowland Havel River, Germany, by agricultural fertilization and effluents of sewage treatment plants. *Applied Geochemistry***,** 62-72.

MORRIS, D. A. & JOHNSON, A. I. 1966. Summary of hydrologic and physical properties of rock and soil materials, as analyzed by the hydrologic laboratory of the U.S. Geological Survey, 1948-60. *Open-File Report.* US Geological Survey.

MRI 2015. Elevation-dependent warming in mountain regions of the world. *Nature Climate Change,* 5**,** 424-430.

MULHOLLAND, P. J. & HILL, W. R. 1997. Seasonal patterns in streamwater nutrient and dissolved organic carbon concentrations: Separating catchment flow path and in-stream effects. *Water Resources Research,* 33**,** 1297-1306.

NATIONAL AUDUBON SOCIETY. 2020. *Unaweep Seep Natural Area* [Online]. Available: https://www.audubon.org/important-bird-areas/unaweep-seep-natural-area [Accessed].

NOACK, C. W., DZOMBAK, D. A. & KARAMALIDIS, A. K. 2014. Rare Earth Element Distributions and Trends in Natural Waters with a Focus on Groundwater. *Environmental Science & Technology,* 48**,** 4317-4326.

NRCS. 2021. Available: https://www.nrcs.usda.gov/Internet/WCIS/AWS_PLOTS/basinCharts/POR/WTEQ/assocHUCco2_8//uncompahgre_plateau.html [Accessed 2021].

O'DRISCOLL, M., DEWALLE, D., HUMPHREY, C. & IVERSON, G. 2019. Groundwater Seeps: Portholes to Evaluate Groundwater's Influence on Stream Water Quality. *Journal of Contemporary Water Research & Education,* 166**,** 57-78.

OGRINC, N., TAMŠE, S., ZAVADLAV, S., VRZEL, J. & JIN, L. 2019. Evaluation of geochemical processes and nitrate pollution sources at the Ljubljansko polje aquifer (Slovenia): A stable isotope perspective. *Science of The Total Environment,* 646**,** 1588-1600.

PALAREA-ALBALADEJO, J., MARTÍN-FERNÁNDEZ, J. A. & OLEA, R. A. 2014. A bootstrap estimation scheme for chemical compositional data with nondetects. *Journal of Chemometrics,* 28**,** 585-599.

PATTERSON, A. 2019. *RELFECTION SEISMIC INVESTIGATION OF AN ALPINE VALLEY IN UNAWEEP CANYON, WESTERN COLORADO: EVIDENCE OF PALEOZOIC GLACIATION OF THE UNCOMPAHGRE PLATEAU*

. Masters, University of Oklahoma.

PLAYÀ, E., CENDÓN, D. I., TRAVÉ, A., CHIVAS, A. R. & GARCÍA, A. 2007. Non-marine evaporites with both inherited marine and continental signatures: The Gulf of Carpentaria, Australia, at ~70 ka. *Sedimentary Geology,* 201**,** 267-285.

POH, S. C. & GASPARON, M. 2011. Rare earth elements: indicators of redox conditions and surface water–groundwater mixing in an estuarine wetland. . *Mineral, Mag.*

POKROVSKY, O. S. & SCHOTT, J. 2002. Surface Chemistry and Dissolution Kinetics of Divalent Metal Carbonates. *Environmental Science & Technology,* 36**,** 426-432.

POURRET, O., DAVRANCHE, M., GRUAU, G. & DIA, A. 2007. Rare earth elements complexation with humic acid. *Chemical Geology,* 243**,** 128-141.

POURRET, O., GRUAU, G., DIA, A., DAVRANCHE, M. & MOLÉNAT, J. 2009. Colloidal Control on the Distribution of Rare Earth Elements in Shallow Groundwaters. *Aquatic Geochemistry,* 16**,** 31-59.

POWELL, J. W. 1879. Report on the lands of the arid region of the United States with a more detailed account of the land of Utah with maps. *Monograph.* US Geological Survey.

RIWAYAT, A. I., AHMAD NAZRI, M. A. & ZAINAL ABIDIN, M. H. 2018. Application of Electrical Resistivity Method (ERM) in Groundwater Exploration. *Journal of Physics: Conference Series,* 995**,** 012094.

RIZZO, E., SUSKI, B., REVIL, A., STRAFACE, S. & TROISI, S. 2004. Self-potential signals associated with pumping tests experiments. *Journal of Geophysical Research: Solid Earth,* 109.

ROLLISON, H. R. 1994. Using Geochemical Data: Evaluation, Presentation, Interpretation. London (Longman Scientific and Technical), 1993. xxvi + 352 pp. Price £24.99 ISBN 0 582 06701 4. *Mineralogical Magazine,* 58**,** 523-523.

SACKS, L. A., HERMAN, J. S., KONIKOW, L. F. & VELA, A. L. 1992. Seasonal dynamics of groundwater-lake interactions at Doñana National Park, Spain. *Journal of Hydrology,* 136**,** 123-154.

SCANLON, T. M., RAFFENSPERGER, J. P. & HORNBERGER, G. M. 2001. Modeling transport of dissolved silica in a forested headwater catchment: Implications for defining the hydrochemical response of observed flow pathways. *Water Resources Research,* 37**,** 1071-1082.

SEFIE, A., ARIS, A. Z., SHAMSUDDIN, M. K. N., TAWNIE, I., SURATMAN, S., IDRIS, A. N., SAADUDIN, S. B. & WAN AHMAD, W. K. 2015. Hydrogeochemistry of Groundwater from Different Aquifer in Lower Kelantan Basin, Kelantan, Malaysia. *Procedia Environmental Sciences,* 30**,** 151-156.

SHAKYA, B. M., NAKAMURA, T., KAMEI, T., SHRESTHA, S. D. & NISHIDA, K. 2019. Seasonal Groundwater Quality Status and Nitrogen Contamination in the Shallow Aquifer System of the Kathmandu Valley, Nepal. *Water,* 11.

SHAW, G. D., MITCHELL, K. L. & GAMMONS, C. H. 2017. Estimating groundwater inflow and leakage outflow for an intermontane lake with a structurally complex geology: Georgetown Lake in Montana, USA. *Hydrogeology Journal,* 25**,** 135-149.

SHILLER, A. M. 1997. Dissolved trace elements in the Mississippi River: Seasonal, interannual, and decadal variability. *Geochimica et Cosmochimica Acta,* 61**,** 4321-4330.

SHILLER, A. M. 2002. Seasonality of dissolved rare earth elements in the lower Mississippi River. *Geochemistry, Geophysics, Geosystems,* 3**,** 1-14.

SHOLKOVITZ, E. R., SHAW, T. J. & SCHNEIDER, D. L. 1992. The geochemistry of rare earth elements in the seasonally anoxic water column and porewaters of Chesapeake Bay. *Geochimica et Cosmochimica Acta,* 56**,** 3389-3402.

SIPPEL, S., MEINSHAUSEN, N., FISCHER, E. M., SZÉKELY, E. & KNUTTI, R. 2020. Climate change now detectable from any single day of weather at global scale. *Nature Climate Change,* 10**,** 35-41.

SMEDLEY, P. L. 1991. The geochemistry of rare earth elements in groundwater from the Carnmenellis area, southwest England. *Geochimica et Cosmochimica Acta,* 55**,** 2767-2779.

SODERBERG, K., GOOD, S. P., O'CONNOR, M., WANG, L., RYAN, K. & CAYLOR, K. K. 2013. Using atmospheric trajectories to model the isotopic composition of rainfall in central Kenya. *Ecosphere,* 4**,** art33.

SOREGHAN, G. S., SOREGHAN, M. J., SWEET, D. E. & MOORE, K. D. 2009. Hot Fan or Cold Outwash? Hypothesized Proglacial Deposition in the Upper Paleozoic Cutler Formation, Western Tropical Pangea. *Journal of Sedimentary Research,* 79**,** 495-522.

SOREGHAN, G. S., SWEET, D. E., THOMSON, S. N., KAPLAN, S. A., MARRA, K. R., BALCO, G. & ECCLES, T. M. 2015. Geology of Unaweep Canyon and its role in the drainage evolution of the northern Colorado Plateau. *Geosphere,* 11**,** 320-341.

SOULSBY, C., MALCOLM, R., HELLIWELL, R. & FERRIER, R. C. 1999. Hydrogeochemsitry of montane springs and their influence on streams in the Cairngorm mountains, Scotland. *Hydrology and Earth System Sciences,* 3**,** 409-419.

TANG, J. & JOHANNESSON, K. H. 2010. Ligand extraction of rare earth elements from aquifer sediments: Implications for rare earth element complexation with organic matter in natural waters. *Geochimica et Cosmochimica Acta,* 74**,** 6690-6705.

TAYLOR, R. G., SCANLON, B., DÖLL, P., RODELL, M., VAN BEEK, R., WADA, Y., LONGUEVERGNE, L., LEBLANC, M., FAMIGLIETTI, J. S., EDMUNDS, M., KONIKOW, L., GREEN, T. R., CHEN, J., TANIGUCHI, M., BIERKENS, M. F. P., MACDONALD, A., FAN, Y., MAXWELL, R. M., YECHIELI, Y., GURDAK, J. J., ALLEN, D. M., SHAMSUDDUHA, M., HISCOCK, K., YEH, P. J. F., HOLMAN, I. & TREIDEL, H. 2013. Ground water and climate change. *Nature Climate Change,* 3**,** 322-329.

TAYLOR, S., FENG, X., KIRCHNER, J. W., OSTERHUBER, R., KLAUE, B. & RENSHAW, C. E. 2001. Isotopic evolution of a seasonal snowpack and its melt. *Water Resources Research,* 37**,** 759-769.

THOMAS, J., JOSEPH, S., THRIVIKRAMJI, K. P., MANJUSREE, T. M. & ARUNKUMAR, K. S. 2014. Seasonal variation in major ion chemistry of a tropical mountain river, the southern Western Ghats, Kerala, India. *Environmental Earth Sciences,* 71**,** 2333-2351.

TORRES-MARTÍNEZ, J. A., MORA, A., MAHLKNECHT, J., DAESSLÉ, L. W., CERVANTES-AVILÉS, P. A. & LEDESMA-RUIZ, R. 2021. Estimation of nitrate pollution sources and transformations in groundwater of an intensive livestock-agricultural

area (Comarca Lagunera), combining major ions, stable isotopes and MixSIAR model. *Environmental Pollution,* 269**,** 115445.

TWEED, S. O., WEAVER, T. R., CARTWRIGHT, I. & SCHAEFER, B. 2006. Behavior of rare earth elements in groundwater during flow and mixing in fractured rock aquifers: An example from the Dandenong Ranges, southeast Australia. *Chemical Geology,* 234**,** 291-307.

UNITED NATIONS ENVIRONMENT PROGRAM 1999. Global environment outlook 2000. Earthscan, UK.

USGS. 2016. *National Water Information System data available on the World Wide Web (USGS Water Data for The Nation)* [Online]. Available: http://waterdata.usgs.gov/nwis/ [Accessed].

USGS. 2021. *Temperature and Water* [Online]. Available: https://www.usgs.gov/special-topic/water-science-school/science/temperature-and-water?qt-science_center_objects=0#qt-science_center_objects [Accessed].

USGS STREAMSTATS. 2016. *The StreamStats program for Colorado* [Online]. Available: http://water.usgs.gov/osw/streamstats/colorado.html, [Accessed].

VALETT, H. M., MORRICE, J. A., DAHM, C. N. & CAMPANA, M. E. 1996. Parent lithology, surface-groundwater exchange, and nitrate retention in headwater streams. *Limnology and Oceanography,* 41**,** 333-345.

VASU, D., SINGH, S. K., TIWARY, P., SAHU, N., RAY, S. K., BUTTE, P. & DURAISAMI, V. P. 2017. Influence of geochemical processes on hydrochemistry and irrigation suitability of groundwater in part of semi-arid Deccan Plateau, India. *Applied Water Science,* 7**,** 3803-3815.

WALTON-DAY, K. & POETER, E. 2009. Investigating hydraulic connections and the origin of water in a mine tunnel using stable isotopes and hydrographs. *Applied Geochemistry,* 24**,** 2266-2282.

WANG, H., JIANG, X.-W., WAN, L., HAN, G. & GUO, H. 2015. Hydrogeochemical characterization of groundwater flow systems in the discharge area of a river basin. *Journal of Hydrology,* 527**,** 433-441.

WEN, X. H., WU, Y. Q. & WU, J. 2007. Hydrochemical characteristics of groundwater in the Zhangye Basin, Northwestern China. *Environmental Geology,* 55**,** 1713-1724.

WIGHTMAN, W. E., JALINOOS, F., SIRLES, P. & HANNA, K. 2003. Application of Geophysical Methods to Highway Related Problems. *In:* FEDERAL HIGHWAY ADMINISTRATION, C. F. L. H. D. (ed.). Lakewood, CO.

WILLIAMS, W. D. 1999. Salinisation: A major threat to water resources in the arid and semi-arid regions of the world. *Lakes and Reservoirs: Research and Management,* 4**,** 85-91.

WINNICK, M. J., CARROLL, R. W. H., WILLIAMS, K. H., MAXWELL, R. M., DONG, W. & MAHER, K. 2017. Snowmelt controls on concentration-discharge relationships and the balance of oxidative and acid-base weathering fluxes in an alpine catchment, East River, Colorado. *Water Resources Research,* 53**,** 2507-2523.

WOOD, S. A. 1990. The aqueous geochemistry of the rare-earth elements and yttrium. *Chemical Geology,* 82**,** 159-186.

YAN, J., MANELSKI, R., VASILAS, B. & JIN, Y. 2018. Mobile Colloidal Organic Carbon: An Underestimated Carbon Pool in Global Carbon Cycles? *Frontiers in Environmental Science,* 6.

YAN, Z., LIU, G., SUN, R., TANG, Q., WU, D., WU, B. & ZHOU, C. 2013. Geochemistry of rare earth elements in groundwater from the Taiyuan Formation limestone aquifer in the Wolonghu Coal Mine, Anhui province, China. *Journal of Geochemical Exploration,* 135**,** 54-62.

YIN, L., HOU, G., SU, X., WANG, D., DONG, J., HAO, Y. & WANG, X. 2011. Isotopes (δD and δ18O) in precipitation, groundwater and surface water in the Ordos Plateau, China: implications with respect to groundwater recharge and circulation. *Hydrogeology Journal,* 19**,** 429-443.

ZEDLER, J. B., MORZARIA-LUNA, H. & WARD, K. 2003. The challenge of restoring vegetation on tidal, hypersaline substrates. *Plant and Soil,* 253**,** 259-273.

ZHANG, B., ZHAO, D., ZHOU, P., QU, S., LIAO, F. & WANG, G. 2020. Hydrochemical Characteristics of Groundwater and Dominant Water–Rock Interactions in the Delingha Area, Qaidam Basin, Northwest China. *Water,* 12**,** 836.

ZHAO, L. J., EASTOE, C. J., LIU, X. H., WANG, L. X., WANG, N. L., XIE, C. & SONG, Y. X. 2018. Origin and residence time of groundwater based on stable and radioactive isotopes in the Heihe River Basin, northwestern China. *Journal of Hydrology: Regional Studies,* 18**,** 31-49.

ZHOU, S., YUAN, X., PENG, S., YUE, J., WANG, X., LIU, H. & WILLIAMS, D. D. 2014. Groundwater-surface water interactions in the hyporheic zone under climate change scenarios. *Environmental Science and Pollution Research,* 21**,** 13943-13955.

Appendix A: Water Chemistry, REE and Isotope data

Table A1. In-situ water chemistry measurements for sampling in 2018 and 2020.

Sample ID	Sample Date	pH	Temp.	Alkalinity	Conductivity	DO	ORP	TDS
		S.U.	°C	mg/L as CaCO3	µS/cm	mg/L	mV	mg/L
UNA-18-1	9/14/18	7.46	11.8	181.96	319	5.9	182	213
UNA-18-1	6/6/20	7.65	11.9	240	389	6.0	240	195
UNA-18-1	8/17/20	7.50	12.1	197	428	6.2	197	215
UNA-18-1	10/6/20	7.36	11.6	225	433	6.3	225	217
UNA-18-4	9/15/18	8.18	13.0	38.41	362	7.5	38	181
UNA-18-4	6/6/20	7.99	16.7	163	377	5.7	163	189
UNA-18-4	10/6/20	7.99	15.6	210	368	7.7	210	184
UNA-18-14	9/15/18	7.29	12.9	70.76	339	4.7	71	170
UNA-18-14	6/6/20	6.98	11.3	266	426	1.2	266	213
UNA-18-14	8/17/20	7.06	11.6	234	408	3.8	234	205
UNA-18-14	10/6/20	6.78	13.9	266	2170	1.5	266	1087
UNA-18-2	9/14/18	7.98	13.2	42.46	293	6.6	194	189
UNA-18-2	6/6/20	8.14	19.6	202	402	7.3	183	201
UNA-18-2	8/17/20	7.98	19.6	233	386	7.6	187	193
UNA-18-2	10/6/20	7.50	11.6	231	416	6.2	196	208

UNA-18-7	9/14/18	8.53	16.3	67.77	331	5.6	194	166
UNA-18-7	6/6/20	8.60	16.6	175	375	6.8	183	188
UNA-18-7	8/17/20	8.51	17.5	184	345	8.0	188	173
UNA-18-7	10/6/20	8.28	8.7	232	376	9.8	195	188
UNA-18-10	9/14/18	8.56	18.7	52.57	277	5.6	187	157
UNA-18-10	6/6/20	8.47	16.9	118	317	6.4	182	158
UNA-18-10	8/17/20	8.43	15.8	167	360	7.1	196	180
UNA-18-10	10/6/20	8.28	9.7	204	368	9.7	191	184
UNA-18-11	9/14/18	7.66	20.2	33.36	2506	3.1	199	1219
UNA-18-11	6/7/20	7.02	15.2	31	2788	3.3	197	1392
UNA-18-11	8/17/20	7.02	21.0	69	2512	2.8	195	1251
UNA-18-11	10/6/20	6.99	14.5	41	2422	4.5	196	1210
UNA-18-12-1	9/14/18	7.74	20.5	56.61	1353	0.0	189	742
UNA-18-12-1	6/7/20	7.67	19.6	115	1563	0.6	177	782
UNA-18-12-1	8/17/20	7.63	21.6	50	1579	0.0	185	789
UNA-18-12-1	10/6/20	7.44	20.2	56.7	1573	0.6	185	790
UNA 19	6/6/20	7.29	11.1	210	324	6.1	192	171
UNA 19	8/17/20	7.19	17.1	202	339	5.9	191	169
UNA 19	10/6/20	6.95	13.1	205	346	6.0	194	173
UNA 20	6/6/20	7.01	12.4	199	425	0.0	190	212

UNA 20	8/17/20	7.00	12.6	181	410	0.0	195	205
UNA 20	10/6/20	6.84	12.0	230	410	0.0	194	205

Table A2. Metal and DOC results (in mg/L) for samples collected in 2018 and 2020. BDL = Below Detection Limit. Dashes indicate no analysis.

Sample ID	**Sample Date**	**DOC (mg C/L)**	**Al**	**As**	**B**	**Ba**	**Ca**	**Cd**	**Cu**	**Cr**	**Fe**	**K**	**Li**	**Mg**
UNA-18-1	9/14/18	-	BDL	BDL	0.03	-	55.8	-	BDL	BDL	BDL	1.6	BDL	8.8
UNA-18-1	6/6/20	0.6	<4	<8	0.02	0.1	58.8	<0.2	<4	<1.1	0	1.1	0.01	10.2
UNA-18-1	8/17/20	0.7	BDL	0.02	0.02	0.1	61.4	0.0003	BDL	BDL	0	1.6	BDL	9.9
UNA-18-1	10/6/20	0.7	BDL	0.03	0.02	0.1	64.9	0.0005	0.02	BDL	0.01	1.6	0	10.2
UNA-18-4	9/15/2018	-	2.32	BDL	0.02	-	52.3	-	BDL	BDL	BDL	1.1	0.01	5.3
UNA-18-4	6/6/20	1	<4	<8	0.02	0.1	55.2	0.0000	<4	<1.1	0.03	1.1	0.01	5.9
UNA-18-4	10/6/20	0.7	BDL	0.02	BDL	0.1	63.7	BDL	BDL	BDL	0.01	1.2	0.01	6.3
UNA-18-14	9/15/18	-	0.21	BDL	0.03	-	49.1	-	BDL	BDL	27.25	1.3	0.01	5.4

UNA-18-14	6/6/20	0.5	<4	0.02	0.05	0.2	61.6	<0.2	<4	<1.1	0.24	1.3	0.01	7.1
UNA-18-14	8/17/20	0.6	BDL	0.02	0.02	0.2	62.8	BDL	BDL	BDL	0	1.9	0.01	7
UNA-18-14	10/6/20	1.9	BDL	0.04	0.02	0.2	76.8	0.0004	BDL	BDL	0.59	2.3	0.01	8.2
UNA-18-2	9/14/18	-	BDL	BDL	0.02	-	49.1	-	BDL	BDL	0.02	1.6	0.01	8
UNA-18-2	6/6/20	4.2	<4	<8	0.02	0.2	56.3	<0.2	<4	<1.1	0.06	2.4	0.02	8.8
UNA-18-2	8/17/20	1.1	BDL	0.02	0.01	0.1	55.3	0.0004	BDL	BDL	0.04	1.4	0.01	9.1
UNA-18-2	10/6/20	1.4	BDL	0.02	0.01	0.1	60.1	0.0004	0.01	BDL	0.03	1.8	0.01	9.2
UNA-18-7	9/14/18	-	0.61	BDL	0.02	-	45.3	-	BDL	BDL	0.06	2.1	0.02	7.3
UNA-18-7	6/6/20	2.5	<4	<8	0.02	0.1	51.4	<0.2	<4	<1.1	0.03	2.1	0.01	8.8
UNA-18-7	8/17/20	1	BDL	0.02	0.01	0.1	47.9	BDL	BDL	BDL	0.01	1.5	0.01	8.2
UNA-18-7	10/6/20	0.9	BDL	0.02	0	0.1	56.3	0.0005	BDL	BDL	0.01	1.6	0.01	8.5
UNA-18-10	9/14/18	-	BDL	BDL	0.03	-	38.4	-	BDL	BDL	0.01	1.8	0.01	6.8
UNA-18-10	6/6/20	2.3	<4	<8	0.02	0.1	44.4	<0.2	<4	<1.1	0.02	1.6	0.01	6.9

UNA-18-10	8/17/20	2.1	BDL	0.02	0.01	0.1	49.9	BDL	BDL	BDL	0	1.6	0.01	8
UNA-18-10	10/6/20	0.9	BDL	0.02	0.01	0.1	54.3	0.0003	BDL	BDL	0	1.7	0.01	7.8
UNA-18-11	9/14/18	-	0.02	0.01	0.61	-	225.1	-	BDL	BDL	0.01	4.7	0.31	0.4
UNA-18-11	6/7/20	0.9	0.08	0.04	0.93	0	250.6	0.0010	<4	<1.1	0.44	4.4	0.42	0.7
UNA-18-11	8/17/20	1.6	BDL	0.06	0.9	0	264.9	0.0007	BDL	BDL	0.2	5.4	0.44	0.6
UNA-18-11	10/6/20	1.1	BDL	0.06	0.82	0	269.2	0.0005	BDL	BDL	0.01	4.2	0.45	0.5
UNA-18-12-1	9/14/18	-	BDL	0	0.62	-	118.2	-	BD	BDL	0.01	3.1	0.13	6
UNA-18-12-1	6/7/20	0.1	<4	0.03	0.82	0	129.8	0.0000	<4	<1.1	0.05	2.2	0.19	6.6
UNA-18-12-1	8/17/20	0.8	BDL	0.03	0.8	0	135.8	0.0005	0.01	BDL	0.04	2.9	0.18	7
UNA-18-12-1	10/6/20	0.2	BDL	0.04	0.8	0	139.2	0.0004	BDL	BDL	0.06	3.2	0.21	7.3
UNA 19	6/6/20	0.1	<4	0.01	0.03	0.1	46.7	<0.2	<4	<1.1	0	1.4	0.01	6.6
UNA 19	8/17/20	0.5	BDL	0.02	0.02	0.1	51.7	0.0003	0.01	BDL	BDL	1.3	0	6.9
UNA 19	10/6/20	0.4	BDL	0.03	0.01	0.2	53.3	0.0006	0.01	BDL	0.13	1.7	0.01	6.8

UNA 20	6/6/20	0.4	<4	0.02	0.02	0.3	58.4	<0.2	<4	<1.1	0.01	1.9	0.01	8.2
UNA 20	8/17/20	0.6	BDL	0.02	0.01	0.2	62.2	BDL	BDL	BDL	0	1.7	BDL	8.3
UNA 20	10/6/20	0.5	BDL	0.02	0.01	0.2	63.6	0.0009	BDL	BDL	0.01	1.9	0.01	8.4

Sample ID	**Sample Date**	**Mn**	**Mo**	**Na**	**Ni**	**P**	**Pb**	**S**	**Se**	**Si**	**Sr**	**Ti**	**Tl**	**V**	**Zn**
UNA-18-1	9/14/18	BDL	BD	9	BDL	0.01	BDL	2.3	BDL	-	0.2	BDL	BDL	BDL	BD
UNA-18-1	6/6/20	<0.1	0	7.5	<1.4	0.02	<6	3.3	<8	9.2	0.3	<0.6	0.01	<3	0.05
UNA-18-1	8/17/20	0	0	8.2	BDL	BDL	BDL	4.3	0.02	9.3	0.3	BDL	BDL	BDL	0
UNA-18-1	10/6/20	0	0	8.2	0.01	0.01	BDL	3.9	0.03	9	0.3	BDL	0.02	BDL	BDL
UNA-18-4	9/15/2018	BDL	BD	6.3	BDL	BD	BDL	2.2	BDL	-	0.2	BDL	BDL	BDL	BD
UNA-18-4	6/6/20	0.01	0	5.4	<1.4	<2	<6	4.1	0.01	8.5	0.2	<0.6	<8	<3	<0.3
UNA-18-4	10/6/20	0.01	0	6.4	0.01	BDL	BDL	3.8	0.02	8.1	0.2	BDL	0.02	BDL	BDL

UNA-18-14	9/15/18	BDL	BD	5.7	BDL	0.05	BDL	2.1	BDL	-	0.2	BDL	BDL	BDL	BDL
UNA-18-14	6/6/20	0.06	0.01	5.8	<1.4	<2	<6	4.6	0.02	7.2	0.2	<0.6	<8	<3	<0.3
UNA-18-14	8/17/20	0	0	5.5	BDL	0.02	BDL	4.9	0.01	7.4	0.2	BDL	0.01	BDL	0
UNA-18-14	10/6/20	0.19	0	7.3	0.01	BDL	BDL	6.9	0.02	6.9	0.3	BDL	0.02	BDL	BDL
UNA-18-2	9/14/18	BDL	BD	7.4	BDL	0.01	BDL	1.6	BDL	-	0.2	BDL	BDL	BDL	BD
UNA-18-2	6/6/20	0.02	0	4.8	<1.4	0.02	<6	2.6	<8	7	0.2	<0.6	<8	<3	0
UNA-18-2	8/17/20	0.01	0	7.3	BDL	0.06	BDL	3.5	0.02	7.8	0.3	BDL	BDL	BDL	0
UNA-18-2	10/6/20	0.02	0	7	0.01	0.01	BDL	3.4	0.03	7.8	0.3	BDL	0.02	BDL	0.01
UNA-18-7	9/14/18	0.01	BD	10.4	BDL	0.17	BDL	2.7	BDL	-	0.2	0.01	BDL	BDL	0.01
UNA-18-7	6/6/20	0.01	0	6.1	<1.4	<2	<6	2.8	<8	7.8	0.2	<0.6	<8	<3	<0.3
UNA-18-7	8/17/20	0	0	7.6	BDL	BDL	BDL	3.6	0.01	7.7	0.2	BDL	BDL	BDL	0.01

UNA-18-7	10/6/20	0	0	7.4	0.01	BDL	BDL	3.3	0.03	7.7	0.2	BDL	0.02	BDL	0
UNA-18-10	9/14/18	BDL	BDL	9.1	BDL	BDL	BDL	3.4	BDL	-	0.2	BDL	BDL	BDL	BD
UNA-18-10	6/6/20	0	0	4.8	<1.4	0.02	<6	2.6	<8	6.3	0.2	<0.6	<8	<3	0.03
UNA-18-10	8/17/20	0	0	7.8	BDL	BDL	BDL	4.3	BDL	7.5	0.3	BDL	0.01	BDL	0
UNA-18-10	10/6/20	0	0	7.4	0.01	BDL	BDL	4	0.01	7.4	0.2	BDL	0.02	BDL	BDL
UNA-18-11	9/14/18	0.01	0.02	216	BDL	0.01	BDL	193.3	BDL	-	3.4	BDL	BDL	BDL	BD
UNA-18-11	6/7/20	0.13	0.02	264.5	<1.4	<2	<6	294.4	0.02	14.5	5	0	0.03	<3	0.01
UNA-18-11	8/17/20	0.06	0.03	236.6	0	BDL	BDL	278.9	0.02	14.9	5.8	BDL	0.03	BDL	0.01
UNA-18-11	10/6/20	0	0.02	226.4	0.01	BDL	BDL	244.7	0.04	13.6	5.9	BDL	0.03	BDL	BDL
UNA-18-12-1	9/14/18	0.02	0.01	133.8	BDL	BD	BDL	118.5	BD	-	2.4	BDL	BDL	BDL	BD
UNA-18-12-1	6/7/20	0.03	0.02	151.1	<1.4	<2	<6	164.7	0.02	9.8	3.3	<0.6	0.02	<3	0.02

UNA-18-12-1	8/17/20	0.03	0.02	140.5	BDL	BDL	BDL	164.4	0.02	9.6	3.7	BDL	0.02	BDL	0.01
UNA-18-12-1	10/6/20	0.03	0.02	139.9	0.01	BDL	BDL	148.6	0.03	9.7	3.7	BDL	0.03	BDL	BDL
UNA 19	6/6/20	<0.1	0	5	<1.4	0.01	<6	3.8	0.02	7.5	0.2	<0.6	<8	<3	0.03
UNA 19	8/17/20	BDL	BDL	4.9	0	0.02	BDL	3.7	0.01	7.9	0.2	BDL	BDL	BDL	0.04
UNA 19	10/6/20	BDL	0	4.8	0.01	0.03	BDL	3.2	0.02	7.8	0.2	BDL	0.02	BDL	0.03
UNA 20	6/6/20	0.57	0	6.4	<1.4	0.01	<6	4.2	<8	6.2	0.3	<0.6	<8	<3	0.05
UNA 20	8/17/20	0.88	0	5.7	BDL	0.01	BDL	4.2	0.01	6.9	0.3	BDL	BDL	BDL	0.04
UNA 20	10/6/20	0.74	0	5.5	0.01	BDL	BDL	3.5	0.04	6.4	0.2	BDL	0.02	BDL	0.02

Table A3. Anion results (mg/L) for samples collected in 2018 and 2020. Values with a "<" in front of them represent concentrations below detection limits.

Sample ID	**Sample Date**	**F^-**	**Cl^-**	**NO_2^-**	**Br^-**	**NO_3^-**	**PO_4^{3-}**	**SO_4^{2-}**	**CO_3^-+ HCO_3^-**
UNA-18-1	9/14/18	0.14	0.9	0.2	<0.10	0.94	<0.5	7.16	3.63
UNA-18-1	6/6/20	0.5	2.0	<0.10	<0.10	0.8	<0.5	7.0	4.72
UNA-18-1	8/17/20	0.5	2.2	<0.10	<0.10	1.0	<0.50	6.0	4.10

UNA-18-1	10/6/20	0.6	2.4	<0.1	<0.1	1.5	<0.5	7.0	8.50
UNA-18-4	9/15/18	0.74	1.18	0.21	<0.10	0.4	<0.5	6.69	0.76
UNA-18-4	6/6/20	0.5	3.5	<0.10	<0.10	0.4	<0.5	6.0	3.38
UNA-18-4	10/6/20	1.0	2.7	<0.1	<0.1	0.5	<0.5	7.0	7.90
UNA-18-14	9/15/18	0.45	1.36	0.24	<0.10	0.36	<0.5	5.6	1.42
UNA-18-14	6/6/20	0.5	3.5	<0.10	<0.10	0.4	<0.5	6.0	4.53
UNA-18-14	8/17/20	0.7	2.8	<0.10	<0.10	3.0	<0.50	9.0	4.87
UNA-18-14	10/6/20	0.7	6.5	<0.1	<0.1	0.4	<0.5	13.3	10.06
UNA-18-2	9/14/18	0.2	2.48	0.19	<0.10	<0.1	<0.5	5.19	0.85
UNA-18-2	6/6/20	0.2	4.0	<0.10	<0.10	<0.10	<0.5	5.0	3.43
UNA-18-2	8/17/20	0.3	3.5	<0.10	<0.10	<0.10	<0.50	5.0	4.62
UNA-18-2	10/6/20	0.3	4.0	<0.1	<0.1	0.2	<0.5	5.8	8.72
UNA-18-7	9/14/18	0.27	2.34	0.18	<0.10	<0.1	<0.5	5.32	1.33
UNA-18-7	6/6/20	0.3	3.6	<0.10	<0.10	<0.10	<0.5	6.0	3.59
UNA-18-7	8/17/20	0.3	3.7	<0.10	<0.10	<0.10	<0.50	6.0	3.78
UNA-18-7	10/6/20	0.5	3.6	<0.1	<0.1	<0.1	<0.5	6.1	8.69
UNA-18-10	9/14/18	0.52	5.27	<0.1	<0.10	<0.1	<0.5	12.54	1.03
UNA-18-10	6/6/20	0.4	3.3	<0.10	<0.10	<0.10	<0.5	6.0	2.30
UNA-18-10	8/17/20	0.6	4.0	<0.10	<0.10	<0.10	<0.50	7.0	3.45
UNA-18-10	10/6/20	0.6	4.2	<0.1	<0.1	<0.1	<0.5	8.1	7.64
UNA-18-11	9/14/18	3.13	382.5	0.63	0.39	<0.1	<0.5	673.5	0.67
UNA-18-11	6/7/20	2.4	286.4	<0.10	1.3	<0.10	<0.5	469	0.61
UNA-18-11	8/17/20	2.7	428	<0.10	1.2	<0.10	<0.50	697	1.44
UNA-18-11	10/6/20	2.4	269.5	<0.1	1.1	<0.1	<0.5	455	1.54
UNA-18-12-1	9/14/18	2.99	178.4	0.41	0.78	<0.1	<0.5	404.8	1.13
UNA-18-12-1	6/7/20	3.1	158.4	<0.10	0.8	<0.10	<0.5	325	2.39
UNA-18-12-1	8/17/20	2.9	189	<0.10	0.7	<0.10	<0.50	409	1.04

UNA-18-12-1	10/6/20	3.0	158.1	<0.1	0.6	<0.1	<0.5	319	2.14
UNA 19	6/6/20	0.5	1.6	<0.10	<0.10	1.0	<0.5	6.0	4.37
UNA 19	8/17/20	0.5	1.1	<0.10	<0.10	1.0	<0.50	6.0	4.20
UNA 19	10/6/20	0.6	1.1	<0.1	<0.1	1.1	<0.5	6.0	7.75
UNA 20	6/6/20	0.1	4.3	<0.10	<0.10	0.6	<0.5	6.0	4.14
UNA 20	8/17/20	0.1	3.5	<0.10	<0.10	2.2	<0.50	6.0	3.77
UNA 20	10/6/20	0.2	2.7	<0.1	<0.1	2.6	<0.5	5.8	8.70

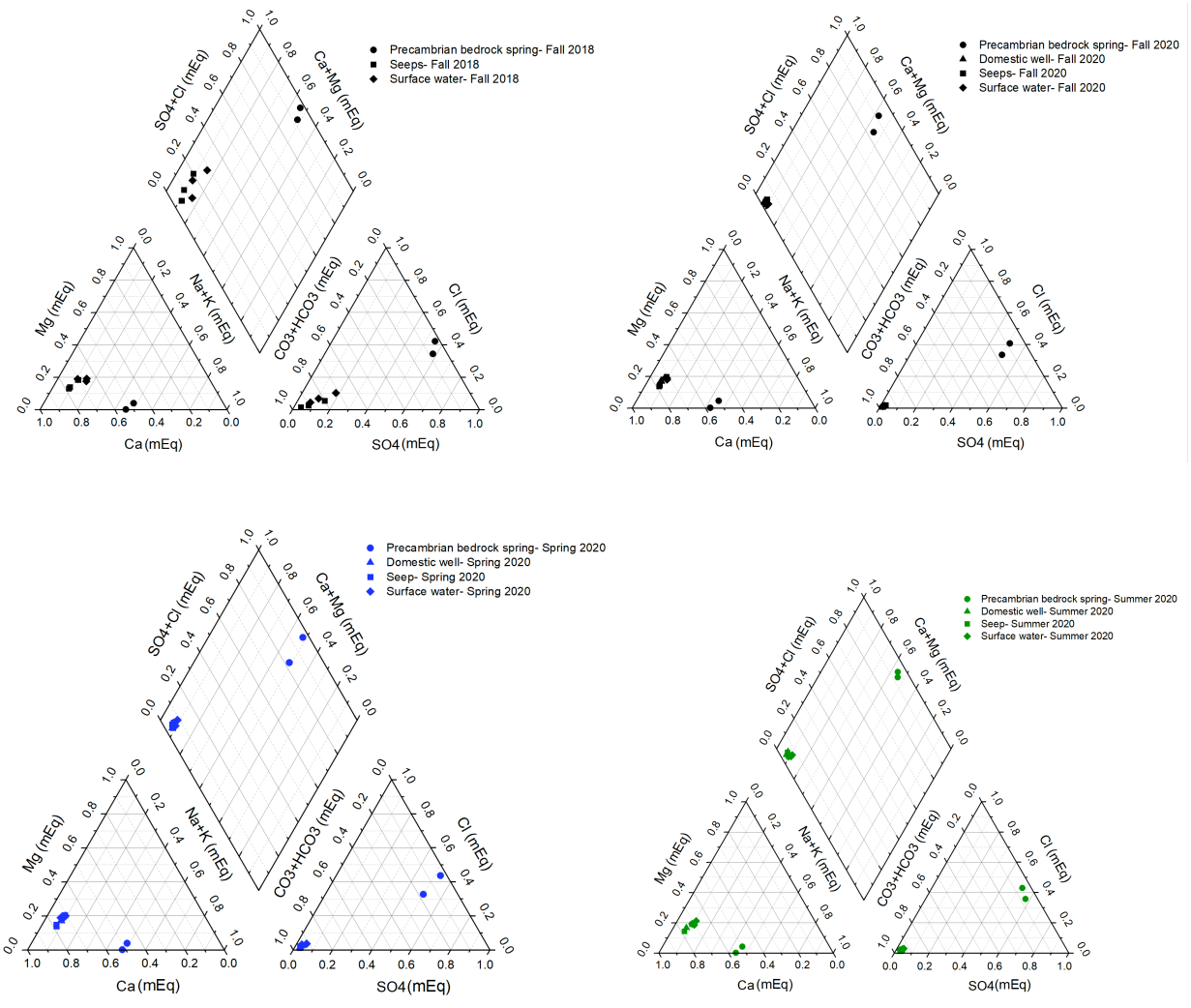

Figure A1. Piper plots of samples collected in 2018 and 2020 representing each sampling season.

Table A4. REE concentrations (ug/L) for samples collected in 2018 and 2020.

Sample ID	Sample Date	Y^{89}	La^{1} 39	Ce^{1} 40	Pr^{1} 41	Nd^{1} 42	Sm 152	Eu^{1} 53	Gd 158	Tb^{1} 59	Dy^{1} 64	Ho^{1} 65	Er^{1} 66	Tm 169	Yb^{1} 74	Lu^{1} 75	Th^{2} 32	U^{23} 8
UNA-18-1	9/14/18	0.0362	0.0658	0.0572	0.0532	0.0433	0.0821	0.0972	0.0761	0.0537	0.0480	0.0570	0.0609	0.0588	0.0590	0.0606	0.0466	7.0700
UNA-18-1	6/6/20	0.0169	0.0051	0.0047	0.0001	0.0001	0.0316	0.0227	0.0001	0.0001	0.0001	0.0001	0.0007	0.0000	0.0006	0.0001	0.0192	5.6200
UNA-18-1	8/17/20	0.0175	0.0023	0.0028	0.0001	0.0001	0.0304	0.0239	0.0001	0.0001	0.0007	0.0022	0.0023	0.0016	0.0009	0.0001	0.0001	6.0100
UNA-18-1	10/6/20	0.0308	0.0074	0.0001	0.0001	0.0045	0.0362	0.0231	0.0001	0.0001	0.0011	0.0001	0.0021	0.0001	0.0036	0.0001	0.0001	6.2900
UNA-18-4	9/15/18	0.0001	0.0451	0.0177	0.0103	0.0195	0.0001	0.0426	0.0093	0.0057	0.0148	0.0064	0.0105	0.0083	0.0075	0.0065	0.0136	3.8400
UNA-18-4	6/6/20	0.0363	0.0223	0.0305	0.0028	0.0175	0.0480	0.0339	0.0044	0.0001	0.0042	0.0001	0.0024	0.0000	0.0033	0.0001	0.0001	2.6300
UNA-18-4	10/6/20	0.0208	0.0019	0.0001	0.0001	0.0001	0.0383	0.0269	0.0001	0.0001	0.0001	0.0001	0.0001	0.0001	0.0004	0.0001	0.0001	4.0300
UNA-18-14	9/15/18	0.0616	0.0001	0.0564	0.0419	0.0001	0.0112	0.0666	0.0264	0.0081	0.0260	0.0138	0.0206	0.0105	0.0088	0.0108	0.0114	1.2400
UNA-18-14	6/6/20	0.0180	0.0001	0.0014	0.0001	0.0001	0.0267	0.0173	0.0001	0.0001	0.0006	0.0001	0.0001	0.0001	0.0001	0.0001	0.0001	5.0000
UNA-18-14	8/17/20	0.0145	0.0046	0.0001	0.0001	0.0002	0.0396	0.0267	0.0001	0.0001	0.0001	0.0001	0.0001	0.0001	0.0001	0.0001	0.0001	3.8100

UNA-18-14	10/6/20	0.0345	0.0130	0.0057	0.0001	0.0015	0.0270	0.0185	0.0001	0.0001	0.0001	0.0001	0.0007	0.0001	0.0022	0.0001	0.0001	3.2500
UNA-18-2	9/14/18	0.0064	0.0741	0.0653	0.0446	0.0627	0.0563	0.0866	0.0417	0.0452	0.0513	0.0494	0.0656	0.0526	0.0473	0.0519	0.0378	4.6800
UNA-18-2	6/6/20	0.0189	0.0111	0.0181	0.0001	0.0062	0.0436	0.0262	0.0021	0.0001	0.0012	0.0001	0.0001	0.0001	0.0008	0.0001	0.0001	3.1700
UNA-18-2	8/17/20	0.0039	0.0001	0.0001	0.0001	0.0001	0.0302	0.0205	0.0001	0.0001	0.0001	0.0001	0.0001	0.0001	0.0001	0.0001	0.0001	3.9400
UNA-18-2	10/6/20	0.0001	0.0001	0.0001	0.0001	0.0001	0.0310	0.0237	0.0001	0.0001	0.0001	0.0001	0.0001	0.0001	0.0001	0.0001	0.0001	4.3700
UNA-18-7	9/14/18	0.2420	0.1840	0.1880	0.2420	0.0001	0.0454	0.0590	0.0943	0.0183	0.1030	0.0169	0.0402	0.0127	0.0308	0.0099	0.0108	4.4500
UNA-18-7	6/6/20	0.0155	0.0078	0.0121	0.0001	0.0037	0.0355	0.0232	0.0001	0.0001	0.0014	0.0001	0.0006	0.0001	0.0013	0.0001	0.0001	2.9200
UNA-18-7	8/17/20	0.0040	0.0001	0.0001	0.0001	0.0001	0.0391	0.0251	0.0001	0.0001	0.0001	0.0001	0.0001	0.0001	0.0001	0.0001	0.0001	4.1100
UNA-18-7	10/6/20	0.0001	0.0001	0.0001	0.0001	0.0001	0.0346	0.0266	0.0001	0.0001	0.0001	0.0001	0.0001	0.0001	0.0001	0.0001	0.0001	4.3700
UNA-18-10	9/14/18	0.0001	0.0217	0.0185	0.0067	0.0203	0.0117	0.0405	0.0092	0.0040	0.0071	0.0056	0.0056	0.0060	0.0031	0.0030	0.0076	4.5700
UNA-18-10	6/6/20	0.1570	0.2750	0.5690	0.0642	0.2250	0.0465	0.0164	0.0552	0.0026	0.0279	0.0058	0.0151	0.0012	0.0106	0.0001	0.0001	0.4290
UNA-18-10	8/17/20	0.1130	0.1590	0.2800	0.0342	0.1390	0.0286	0.0122	0.0325	0.0001	0.0170	0.0028	0.0096	0.0001	0.0077	0.0001	0.0001	0.3690
UNA-18-10	10/6/20	0.0517	0.0229	0.0001	0.0001	0.0001	0.0057	0.0037	0.0001	0.0001	0.0021	0.0001	0.0001	0.0001	0.0009	0.0001	0.0001	0.3790
UNA-18-11	9/14/18	0.0062	0.0440	0.0632	0.0126	0.0330	0.0145	0.0136	0.0064	0.0066	0.0180	0.0076	0.0053	0.0055	0.0025	0.0050	0.0160	0.8610
UNA-18-11	6/7/20	0.0322	0.0016	0.0006	0.0001	0.0001	0.0049	0.0044	0.0001	0.0001	0.0007	0.0001	0.0001	0.0001	0.0001	0.0001	0.0001	0.4810

UNA-18-11	8/17/20	0.0267	0.001	0.001	0.001	0.001	0.033	0.029	0.001	0.001	0.001	0.001	0.001	0.001	0.001	0.001	0.001	0.940
UNA-18-11	10/6/20	0.0337	0.022	0.001	0.001	0.001	0.074	0.042	0.001	0.001	0.001	0.001	0.001	0.001	0.001	0.001	0.001	0.850
UNA-18-12-1	9/14/18	0.001	0.165	0.305	0.162	0.174	0.072	0.155	0.194	0.132	0.172	0.146	0.168	0.146	0.140	0.139	0.122	0.580
UNA-18-12-1	6/7/20	0.611	0.151	0.113	0.011	0.134	0.707	0.468	0.037	0.001	0.051	0.008	0.014	0.001	0.025	0.001	0.001	1.600
UNA-18-12-1	8/17/20	0.840	0.239	0.001	0.032	0.165	0.635	0.428	0.003	0.001	0.014	0.001	0.029	0.001	0.027	0.001	0.001	1.200
UNA-18-12-1	10/6/20	0.067	0.059	0.001	0.001	0.001	0.586	0.441	0.001	0.001	0.001	0.001	0.001	0.001	0.001	0.001	0.001	0.660
UNA 19	6/6/20	0.576	0.065	0.001	0.001	0.034	0.474	0.259	0.001	0.001	0.033	0.001	0.019	0.001	0.029	0.001	0.001	2.700
UNA 19	8/17/20	0.462	0.016	0.001	0.001	0.001	0.470	0.317	0.001	0.001	0.023	0.001	0.006	0.001	0.003	0.001	0.001	3.300
UNA 19	10/6/20	0.593	0.078	0.080	0.005	0.025	0.404	0.314	0.038	0.001	0.021	0.001	0.035	0.001	0.014	0.001	0.001	3.1800
UNA 20	6/6/20	0.197	0.045	0.001	0.001	0.001	0.899	0.560	0.001	0.001	0.001	0.001	0.001	0.001	0.001	0.001	0.001	2.200
UNA 20	8/17/20	0.193	0.035	0.001	0.001	0.001	0.757	0.512	0.001	0.001	0.001	0.001	0.001	0.001	0.001	0.001	0.001	2.7500
UNA 20	10/6/20	0.323	0.057	0.115	0.001	0.034	0.729	0.493	0.001	0.001	0.018	0.001	0.006	0.001	0.012	0.001	0.001	2.6400

Appendix B. PCA Plot data

Table B1. Data for from PCA and development of the PCA plot.

Sample ID	Sample Date	PC 1 (58.41%)	PC 2 (23.11%)
UNA-18-1	6/6/20	1.29	-1.33
UNA-18-1	10/6/20	0.75	-1.78
UNA-18-4	6/6/20	0.14	-0.91
UNA-18-4	10/6/20	0.80	0.49
UNA-18-14	6/6/20	0.77	-0.06
UNA-18-14	8/17/20	0.43	-0.46
UNA-18-14	10/6/20	0.91	-0.48
UNA-18-2	6/6/20	3.05	3.64
UNA-18-2	8/17/20	1.28	-0.25
UNA-18-2	10/6/20	0.61	-1.13
UNA-18-7	6/6/20	1.86	1.73
UNA-18-7	8/17/20	0.59	-0.53
UNA-18-7	10/6/20	0.30	-1.07
UNA-18-10	6/6/20	1.59	1.97

UNA-18-10	8/17/20	0.78	0.39
UNA-18-10	10/6/20	-4.23	0.49
UNA-18-11	6/7/20	-3.60	1.16
UNA-18-11	8/17/20	-4.08	0.75
UNA-18-11	10/6/20	-2.76	0.05
UNA-18-12-1	6/7/20	-1.87	0.22
UNA-18-12-1	8/17/20	-2.42	0.75
UNA-18-12-1	10/6/20	0.04	-1.22
UNA 19	6/6/20	0.44	-1.01
UNA 19	8/17/20	0.12	-1.06
UNA 19	10/6/20	1.08	-0.33
UNA 20	6/6/20	1.27	-0.01
UNA 20	8/17/20	0.86	-0.01

Table B2. Loading values for each loading component for the PCA plots

	PC 1 (58.41%)	**PC 2 (23.11%)**
D18O	0.39875	0.45865
D2H	0.506	0.1795
Alkalinity	0.43575	-0.33453
DOC	0.18682	0.65657
Uranium	0.33682	-0.40002

Major Cations	-0.49672	0.23326

Table B3. Complete Spearman's correlation table with both r and p values.

	Spearman's Correlation				
	Spring	**Summer**	**Fall**	**Precambrian bedrock**	**Surface water+ Domestic well+ Seeps**
δ18O - δ2H	0.88091	0.90676	0.90014	0.87537	0.92392
p-value	7.60E-04	0.00189	9.38E-04	0.02233	2.29E-09
δ18O - Alkalinity	0.24479	0.59856	0.71776	0.39446	-0.29338
p-value	0.49548	0.11695	0.02945	0.43899	0.19679
δ18O - DOC	0.80254	-0.23037	0.04309	-0.76536	0.64641
p-value	0.0052	0.5831	0.91234	0.07612	0.00154
δ18O - Uranium	0.0126	0.64725	0.23865	0.84099	-0.3315
p-value	0.97244	0.08275	0.53631	0.03592	0.14211
δ18O - Major Cations	-0.44732	-0.82349	-0.73666	-0.66601	-0.11647
p-value	0.1949	0.01199	0.02358	0.14869	0.61513
δ2H - Alkalinity	0.5522	0.87034	0.9303	0.48263	-0.16114
p-value	0.0979	0.00493	2.75E-04	0.33226	0.4853
δ2H - DOC	0.63825	-0.32635	0.24139	-0.81103	0.59696
p-value	0.04705	0.43016	0.53151	0.05019	0.00428

δ2H - Uranium	0.28196	0.71734	0.40917	0.97044	-0.5038
p-value	0.42996	0.04517	0.27416	0.0013	0.01989
δ2H - Major Cations	-0.77395	-0.94751	-0.89348	-0.92857	0.0182
p-value	0.00861	3.47E-04	0.00117	0.00747	0.9376
Alkalinity - DOC	-0.03737	-0.28517	0.39273	-0.46292	-0.32917
p-value	0.91837	0.49359	0.29577	0.35522	0.1451
Alkalinity - Uranium	0.37618	0.68443	0.60161	0.29082	-0.25255
p-value	0.28401	0.06114	0.08655	0.57607	0.26938
Alkalinity - Major Cations	-0.79104	-0.84354	-0.91632	-0.47777	0.716
p-value	0.00643	0.00849	5.14E-04	0.33787	2.62E-04
Uranium - Major Cations	-0.60379	-0.79989	-0.67679	-0.83247	-0.09184
p-value	0.06454	0.01715	0.04526	0.03975	0.69217
DOC - Uranium	0.11987	0.18153	-0.073	0.83607	-0.08613
p-value	0.74153	0.66703	0.85194	0.03811	0.71047
DOC - Major Cations	-0.23753	0.26797	-0.07858	-0.92461	-0.13147
p-value	0.50875	0.52109	0.84074	0.00831	0.57001

Appendix C. Pictures

Figure 1. Precambrian bedrock spring

Figure 2. West Creek

Figure 3. Domestic Well.

Figure 4. Unaweep seep.

Figure 5. Another Seep in the canyon.